

# Optical response of alternating twisted trilayer graphene

Dionisios Margetis<sup>1,\*</sup> and Tobias Stauber<sup>2,†</sup>

<sup>1</sup>*Department of Mathematics, and Institute for Physical Science and Technology,  
University of Maryland, College Park, Maryland 20742, USA*

<sup>2</sup>*Instituto de Ciencia de Materiales de Madrid, CSIC, E-28049 Madrid, Spain*

(Dated: September 9, 2024)

We study via microscopic considerations and symmetry principles the optical response of the alternating twisted trilayer graphene. The layer-resolved optical conductivities are expressed in terms of contributions from *effective* twisted bilayer and single-layer systems along with their coupling. We show the *emergence* of constitutive laws for: (i) an in-plane magnetic response proportional to the above coupling; and (ii) an *effective* twisted-bilayer electro-magnetic response that involves a chirality parameter. We estimate the in-plane magnetic response to be negligible, but finite for twists close to the magic angle near charge neutrality. Our approach makes use of a unitary transformation for the trilayer Hamiltonian, and the Kubo formulation of linear response theory. We discuss other implications of our analytical results such as features of bulk plasmonic modes.

## I. INTRODUCTION

In 2018, it was shown that the twist angle between two graphene layers can be tuned so that correlated insulator phases<sup>1</sup> and (probably) unconventional superconductivity<sup>2</sup> emerge for small carrier densities around charge neutrality. Other interesting phases such as anomalous Hall ferromagnetism<sup>3,4</sup> or fractional Chern numbers have also been observed.<sup>5–7</sup> These phenomena are related to the flat bands around charge neutrality that have been predicted theoretically.<sup>8,9</sup>

Since then, the study of twisted geometries of van der Waals heterostructures, often referred to as moiré materials,<sup>10</sup> has become an active area of research. The subjects of these investigations include twisted bilayers composed of various transition metal dichalcogenides,<sup>11–18</sup> besides the twisted bilayer graphene. Moreover, the number of sheets in moiré graphene systems has been increased to up to five alternately twisted layers.<sup>19,20</sup> Recently, epitaxially grown quasi-three-dimensional twisted structures were fabricated, which exhibit an intrinsic enhanced chirality.

Lately, special emphasis has been placed on the study of the twisted trilayer graphene.<sup>21–38</sup> This is the minimal system that can form not only quasi-commensurate but also incommensurate structures. Quasi-commensurate structures can be described by two moiré vectors, whereas incommensurate structures are usually described by four moiré vectors - two for each of the moiré lattices that are formed by the two pairs of consecutive layers (say, layers 1 and 2, and layers 2 and 3, respectively).<sup>25,39–41</sup> Interestingly, superconductivity has been found in both types of structures, that is, commensurate<sup>21–23,38</sup> and incommensurate trilayer structures.<sup>42,43</sup>

In this paper, we study analytically the electromagnetic response of the twisted trilayer graphene via symmetry considerations and microscopic principles of linear response theory. We focus on the alternating-twist

configuration, in which  $\theta_{12} = -\theta_{23}$  where  $\theta_{ij}$  denotes the angle between layers  $i$  and  $j$ . In this case, in the presence of mirror symmetry with respect to the central layer, which is also preserved after taking into account in-plane and out-of-plane relaxation,<sup>44</sup> we show that the response of the system can be decomposed into two parts: (i) an effective electro-magnetic response, in which a chirality parameter plays a key role; and (ii) an in-plane magnetic response.

In our analysis, we make use of a unitary transformation, introduced in Ref. 45, that converts the trilayer system into a combination of effective twisted bilayer and single-layer systems. Linear response theory for the trilayer eventually couples these two systems. We derive a formula for this coupling, and estimate its magnitude. We also describe, in terms of contributions from these two systems, the layer-resolved conductivities that enter the optical response in regard to items (i) and (ii) above. In particular, we analytically show how the in-plane magnetic response arises from the coupling of the two effective systems. This approach enables us to assess that the in-plane magnetic response is very weak, but finite for twists close to the magic angle near charge neutrality. In addition, we discuss the Drude weights of bulk plasmonic modes related to the effective electro-magnetic response.

The alternating-twist trilayer system under mirror symmetry investigated here is one of the most stable layered structures, minimizing the configuration stacking fault energy. This remarkable mechanical stability renders this system prototypical, and is another motivation for our work. Note that we extend the analysis for the optical conductivity to alternating-twist trilayers in which the mirror symmetry with respect to the middle layer is broken because of the different inter-layer tunneling. However, this setting is somewhat impractical, since it still retains the condition  $\theta_{12} = -\theta_{23}$  on the twist angles. On the other hand, the interesting case of the optical response for the perturbed alternat-

ing twisted trilayer, in which one of the twist angles changes slightly while interlayer hopping occurs non-symmetrically, is not addressed here.

A highlight of our results is the connection of the phenomenological optical response of the trilayer system, which can be derived from symmetry principles, to microscopic parameters of effective Hamiltonians for simpler systems. Thus, we are able to illustrate the important role of the large moiré length. For example, the effect of this scale renders negligible the relative contribution of the in-plane magnetic response. In this paper, we focus on analytical predictions that explicitly reveal the interplay of two scales in the optical response. Hence, we choose not to use or rely on numerical simulations in this work.

We alert the reader that the term “effective” is used with a twofold meaning. We write “effective system” (or, “effective Hamiltonian”) to mean the twisted bilayer or single-layer Hamiltonian that comes from the unitary transformation of the trilayer system.<sup>45</sup> However, the term “effective response” implies the optical response in items (i) and (ii) above.

The remainder of the paper is organized as follows. In Sec. II, we describe the optical response of the alternating twisted trilayer system by making symmetry-based assumptions on its conductivity tensor. We highlight the emergence of two types of optical responses, their parametrization, and some of their implications. Section III focuses on the structure of the conductivity tensor via the Kubo formulation. In particular, we discuss the roles of the effective twisted bilayer and single-layer systems; and thereby estimate the in-plane magnetic response of the trilayer system. In Sec. IV, we conclude the paper with a summary of our main results. The appendices mainly provide technical derivations relevant to the main text.

Throughout the paper, boldface symbols denote vectors or matrices that pertain to the spatial ( $x$ - and  $y$ -) directions of the reference plane. The symbols  $|\psi\rangle$  and  $\psi$  are employed interchangeably for the eigenvectors of the trilayer Hamiltonian. The  $e^{-i\omega t}$  time dependence is assumed for time harmonic fields ( $\omega$  is the frequency).

## II. TRILAYER OPTICAL RESPONSE

In this section, we describe phenomenological aspects of the optical response. We focus on key constitutive laws of the trilayer system by making symmetry-based assumptions on its layer-resolved conductivities.

The general layer-resolved response theory in the frequency domain for a system with  $n$  layers is given by

$$\mathbf{J}^\ell = \sum_{\ell'=1}^n \boldsymbol{\sigma}^{\ell\ell'} \mathbf{E}_{\ell'} \quad (\ell = 1, \dots, n), \quad (1)$$

where  $\mathbf{J}^\ell$  and  $\mathbf{E}_\ell$  denote the (average) macroscopic surface current density and electric field in sheet  $\ell$ , respectively. The  $2 \times 2$  matrices  $\boldsymbol{\sigma}^{\ell\ell'}(\omega)$  have elements defined by  $\sigma_{\nu\nu'}^{\ell\ell'}(\omega) = i \frac{e^2}{\omega + i\delta} \chi_{\nu\nu'}^{\ell\ell'}(\omega + i\delta)$ , as  $\delta \downarrow 0$ , with the current-current response function

$$\chi_{\nu\nu'}^{\ell\ell'}(\omega) = -\frac{i}{\hbar} \int_0^\infty dt e^{i\omega t} \langle [j_\nu^\ell(t), j_{\nu'}^{\ell'}(0)] \rangle, \quad (2)$$

where  $j_\nu^\ell(t)$  is the  $\nu$ -directed current operator in layer  $\ell$  in the interaction picture, and  $\langle \cdot \rangle$  is a normalized averaging process involving an appropriate trace ( $\ell, \ell' = 1, \dots, n$  and  $\nu, \nu' = x, y$ ); see Sec. III.

We will discuss the case of  $n = 3$  layers under mirror symmetry. The Hamiltonian of the trilayer system along with its unitary transformation into a direct sum of effective twisted bilayer and single-layer systems are reviewed in Appendix A; see also Ref. 45.

### A. Normal modes

The geometry of the alternating-twist trilayer system is shown in Fig. 1. The twist angle of layer  $\ell$  is  $(-1)^\ell \theta/2$  where  $0 < \theta < \pi/2$  and  $\ell = 1, 2, 3$ . The interlayer distance is  $a/2$ .

We consider a mirror-symmetric configuration. Hence, the matrices  $\boldsymbol{\sigma}^{\ell\ell'}$  satisfy  $\boldsymbol{\sigma}^{11} = \boldsymbol{\sigma}^{33}$ ,  $\boldsymbol{\sigma}^{12} = \boldsymbol{\sigma}^{32}$ , and  $\boldsymbol{\sigma}^{21} = \boldsymbol{\sigma}^{23}$ . Time reversal symmetry implies  $\sigma_{\nu\nu'}^{\ell\ell'} = \sigma_{\nu'\nu}^{\ell'\ell}$ ; see Appendix B.

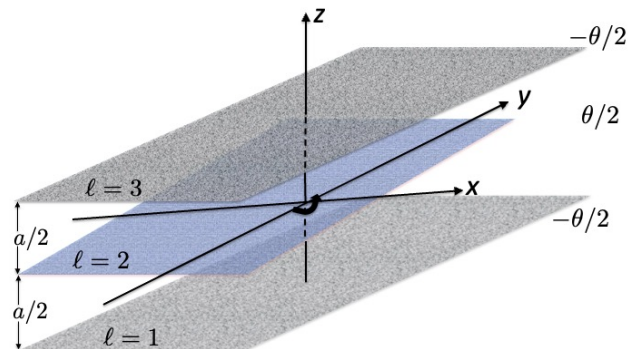


FIG. 1. Schematic of the alternating-twist trilayer configuration. Three infinite flat graphene sheets labeled by  $\ell = 1, 2, 3$  are parallel to the  $xy$ -plane, and have twist angles  $(-1)^\ell \theta/2$  and interlayer distance equal to  $a/2$  ( $0 < \theta < \pi/2$ ). The layers are immersed in a homogeneous medium.

Let us first assume that each of these matrices is proportional to the  $2 \times 2$  identity matrix,  $\boldsymbol{\sigma}^{\ell\ell'} = \sigma_0^{\ell\ell'} \mathbf{1}$ . Hence, there are three eigenmodes, labeled by  $m = -1, 0, 1$ , with current densities  $\mathcal{J}_m$  and electric fields  $\boldsymbol{\mathcal{E}}_m$  such that

$$\mathcal{J}_m = \sigma_m \boldsymbol{\mathcal{E}}_m, \quad (3)$$

where  $2\sigma_{\pm} = \sigma_0^{\pm} \pm \sqrt{8(\sigma_0^{12})^2 + (\sigma_0^{-})^2}$ ,  $\sigma_0 = \sigma_0^{11} - \sigma_0^{13}$ , and  $\sigma_0^{\pm} = \sigma_0^{11} + \sigma_0^{13} \pm \sigma_0^{22}$ . The normal-mode electric field ( $\mathcal{E}_+$ ,  $\mathcal{E}_0$ ,  $\mathcal{E}_-$ ) is related to the original electric field by a simple harmonic model, viz.,

$$\begin{pmatrix} \mathcal{E}_+ \\ \mathcal{E}_0 \\ \mathcal{E}_- \end{pmatrix} = \mathbf{M} \begin{pmatrix} \mathbf{E}_1 \\ \mathbf{E}_2 \\ \mathbf{E}_3 \end{pmatrix}, \quad (4)$$

with

$$\mathbf{M} = \begin{pmatrix} 1 & \alpha_- & 1 \\ -1 & 0 & 1 \\ 1 & -\alpha_+ & 1 \end{pmatrix}. \quad (5)$$

In the above matrix, each entry expresses a  $2 \times 2$  block matrix and the parameters  $\alpha_{\pm}$  are given by

$$\alpha_{\pm} = \frac{\pm\sigma_0^- + \sqrt{8(\sigma_0^{12})^2 + (\sigma_0^-)^2}}{2\sigma_0^{12}}. \quad (6)$$

The original current densities are transformed in the same fashion as the original electric fields in Eq. (4), i.e.,  $\mathcal{J} = \mathbf{M}\mathbf{J}$  where

$$\mathcal{J} = \begin{pmatrix} \mathcal{J}_+ \\ \mathcal{J}_0 \\ \mathcal{J}_- \end{pmatrix}, \quad \mathbf{J} = \begin{pmatrix} \mathbf{J}^1 \\ \mathbf{J}^2 \\ \mathbf{J}^3 \end{pmatrix}.$$

In the presence of chirality, we set  $\sigma^{12} = \sigma_0^{12}\mathbf{1} + i\sigma_{xy}^{12}\tau_y$  where  $\tau_y$  denotes the  $y$ -Pauli matrix and  $\sigma_{xy}^{12}$  is the chirality parameter. There are respective off-diagonal terms for chirality in  $\sigma^{21}$ ,  $\sigma^{23}$  and  $\sigma^{32}$ . By symmetry, we must still have  $\sigma^{13} = \sigma_0^{13}\mathbf{1}$  in this case. Thus, after some manipulation of Eq. (1) we obtain the following coupled system of the optical response:

$$\begin{aligned} \mathcal{J}_+ &= \sigma_+\mathcal{E}_+ + \alpha_-\sigma_{xy}^{12}(\mathbf{e}_z \times \mathcal{E}_-), \\ \mathcal{J}_0 &= \sigma_0\mathcal{E}_0, \\ \mathcal{J}_- &= \sigma_-\mathcal{E}_- - \alpha_+\sigma_{xy}^{12}(\mathbf{e}_z \times \mathcal{E}_+), \end{aligned} \quad (7)$$

where  $\mathbf{e}_z$  is the  $z$ -directed Cartesian unit vector. Note that the response to the field  $\mathcal{E}_0$  remains decoupled from the other modes because  $\sigma^{13} = \sigma_0^{13}\mathbf{1}$ . This is reasonable since in the alternating-twist geometry layers 1 and 3 have the same orientation (see Fig. 1).

The derivation of the normal modes for the alternating twisted trilayer graphene here makes use of symmetry considerations for the structure of the conductivity matrices  $\sigma^{\ell\ell'}$ . To parametrize this structure minimally, we will apply a unitary transformation that reduces the trilayer Hamiltonian to a direct sum of effective single-layer and twisted bilayer Hamiltonians (Appendix A).<sup>45</sup> In this way, we will link  $\sigma^{\ell\ell'}$  to conductivities of effective twisted bilayer and single-layer systems. We will also show the appearance of a mixing term in  $\sigma^{11}$  and  $\sigma^{13}$ , which couples these two effective systems. The related procedure is discussed in Sec. III.

## B. In-plane magnetic response

Equation (7) describes the total optical response of a mirror-symmetric trilayer configuration (Fig. 1). We repeat at the risk of redundancy that, interestingly, one eigenmode (for  $\mathcal{J}_0$ ) decouples from the other modes even in the presence of the chiral parameter,  $\sigma_{xy}^{12}$ . We can thus rewrite the corresponding equation in terms of a magnetic field,  $\mathbf{B}_{\parallel}$ , which gives rise to an in-plane magnetic-dipole moment,  $\mathbf{m}_{\parallel}$ . Following Ref. 46, we define  $\mathbf{m}_{\parallel} = a\mathcal{J}_0 \times \mathbf{e}_z$  where  $a$  is the distance between layers 1 and 3 (Fig. 1). We can also define this magnetic field by writing  $i\omega a\mathbf{B}_{\parallel} = \mathcal{E}_0 \times \mathbf{e}_z$  and invoking Maxwell's equations, where  $\mathbf{B}_{\parallel}$  is the average parallel component of the magnetic field between layer 1 and 3. Thus, we derive the following constitutive law:

$$\mathbf{m}_{\parallel} = i\omega \frac{a^2}{2}(\sigma_0^{11} - \sigma_0^{13})\mathbf{B}_{\parallel}. \quad (8)$$

We will show below that the response parameter  $\sigma_0^{11} - \sigma_0^{13}$  of Eq. (8) can be expressed as a coupling between effective single-layer and twisted bilayer systems (Sec. III B). Mainly because of the kinematic constraints arising from the largely different Fermi velocities in these two systems, this coupling is practically negligible, although still finite (Sec. III C). The fact that the response is finite can be traced back to the discreteness of the layers since the general expression for the in-plane magnetization within the continuum description vanishes.<sup>47</sup>

The small, almost vanishing in-plane magnetic response of twisted trilayer graphene is in stark contrast to the large in-plane magnetic response of twisted bilayer graphene<sup>46</sup> which can even diverge and give rise to a Condon instability.<sup>48,49</sup> Let us also note that in Eq. (8) there is no coupling between the magnetic moment,  $\mathbf{m}_{\parallel}$ , and an in-plane electric field, again unlike the case of the twisted bilayer system.<sup>46</sup>

## C. Effective electro-magnetic response: Constitutive equations

Let us now discuss the remaining two modes, which are coupled by the chiral parameter,  $\sigma_{xy}^{12}$ . Following Ref. 46, we write the *effective* moments as  $-2i\omega\mathbf{p}_{\parallel}^{eff} = \alpha_+\mathcal{J}_+$  for the electric-dipole moment and  $2\mathbf{m}_{\parallel}^{eff} = a\alpha_-\mathcal{J}_- \times \mathbf{e}_z$  for the in-plane magnetic-dipole one. The respective *effective* electric and magnetic fields are given by  $\mathbf{E}_{\parallel}^{eff} = \mathcal{E}_+$  and  $i\omega a\mathbf{B}_{\parallel}^{eff} = \mathcal{E}_- \times \mathbf{e}_z$ . The resulting constitutive equations in matrix form read

$$\begin{pmatrix} \mathbf{p}_{\parallel}^{eff} \\ \mathbf{m}_{\parallel}^{eff} \end{pmatrix} = \begin{pmatrix} \chi_e & G \\ -G & \chi_m \end{pmatrix} \begin{pmatrix} \mathbf{E}_{\parallel}^{eff} \\ \mathbf{B}_{\parallel}^{eff} \end{pmatrix}, \quad (9)$$

which resembles the optical response of the twisted bilayer configuration.<sup>46</sup> In the above, we introduce the following *effective* parameters: electric polarizability  $\chi_e$ , magnetic susceptibility  $\chi_m$ , and electro-magnetic coupling  $G$ . These parameters are related to the layer-resolved sheet conductivities of Sec. II A by

$$\chi_e = -\frac{\alpha_+\sigma_+}{2i\omega}, \quad \chi_m = i\omega\frac{a^2}{2}\alpha_-\sigma_-, \quad G = a\sigma_{xy}^{12}. \quad (10)$$

On the other hand, it is known that the linear response of the twisted bilayer system is characterized by three response functions given by the in-sheet conductivity  $\sigma_0$ , the covalent drag  $\sigma_1$ , and the chiral drag  $\sigma_{xy}$ . Identifying the distance  $a$  between layers 1, 3 with the effective interlayer distance of the bilayer, we set<sup>46</sup>

$$\chi_e = -2\frac{\sigma_0 + \sigma_1}{i\omega}, \quad \chi_m = i\omega\frac{a^2}{2}(\sigma_0 - \sigma_1), \quad G = a\sigma_{xy}.$$

Hence, we establish a mapping of  $(\sigma_+, \sigma_-, \sigma_{xy}^{12})$  to  $(\sigma_0, \sigma_1, \sigma_{xy})$ , expressed by the following equations:

$$\sigma_0 = \frac{1}{8}(\alpha_+\sigma_+ + 4\alpha_-\sigma_-), \quad (11)$$

$$\sigma_1 = \frac{1}{8}(\alpha_+\sigma_+ - 4\alpha_-\sigma_-), \quad (12)$$

$$\sigma_{xy} = \sigma_{xy}^{12}. \quad (13)$$

Recall that each of the parameters  $\alpha_{\pm}$  implicitly depends on  $\sigma_+$  and  $\sigma_-$  via  $\sigma_0^+$  and  $\sigma_0^-$ , for fixed  $\sigma_0^{12}$ . Therefore, Eqs. (11) and (12) describe a nonlinear mapping from the alternating trilayer response parameter space to an effective twisted-bilayer-type response.

Let us invert the system of Eqs. (11) and (12). For this task, we define the dimensionless quantity

$$\varkappa = \frac{1}{2} \frac{5\sigma_0 + 3\sigma_1}{\sqrt{2(\sigma_0 - \sigma_1 + 2\sigma_0^{12})(\sigma_0 + \sigma_1 - \frac{1}{2}\sigma_0^{12})}}. \quad (14)$$

The desired inverse mapping is then expressed by

$$\sigma_{\pm} = \pm\varkappa\sigma_0^{12} + \sqrt{(\varkappa\sigma_0^{12})^2 + 2(\sigma_0^2 - \sigma_1^2)}, \quad (15)$$

after some algebra. Notice that if  $|\varkappa|$  is large, the parameters  $\sigma_+$  and  $\sigma_-$  assume very different values, i.e.,  $\sigma_{\pm} \propto \varkappa^{\pm 1}$ . We see that  $|\sigma_0^{11} + \sigma_0^{13} - \sigma_0^{22}|$  must be much larger than  $|\sigma_0^{12}|$  in this case. This situation may arise when Eq. (14) is singular; thus, either the counterflow conductivity  $\sigma_0 - \sigma_1 \simeq -2\sigma_0^{12}$ , or the total conductivity  $2(\sigma_0 + \sigma_1) \simeq \sigma_0^{12}$ . By appropriate doping, both resonances should be realizable.

#### D. Bulk plasmonic modes

Our eigenmode analysis allows us to discuss the bulk plasmonic modes of the trilayer system. Since the true

magnetic response of Sec. II B is deemed as negligible, we only focus on the implications of the effective electro-magnetic response of Sec. II C. The related case of plasmonic modes for the actual, twisted bilayer system was first discussed in Ref. 46. Two modes were obtained, namely, one optical mode with dispersion  $\omega_+^2 \sim D_+q$  and one acoustic mode with dispersion  $\omega_- \sim D_-q$ , where  $q$  is the wave number and  $D_{\pm}$  denote the related Drude weights.<sup>46</sup>

By relying on the mapping of Eqs. (11)–(13), we now obtain the following Drude weight for the optical mode:

$$D_+ = \lim_{\omega \rightarrow 0} \{\omega \text{Im}(\frac{1}{2}\alpha_+\sigma_+)\}. \quad (16)$$

This *effective* Drude weight will not lead to a “true” oscillating dipole moment, but an *effective* oscillating dipole moment (defined above) instead. The oscillating current density on the outer layers is thus different from the oscillating current density in the middle layer. Equation (16) can be expressed in terms of Kubo formulas for conductivity parameters of effective systems (Sec. III B).

The above Drude weight,  $D_+$ , and thus the dispersion relation of the charge oscillation, does not depend on the chiral response – just as is the case in the actual, real bilayer system. However, the plasmon is chiral; and the *effective* magnetic-dipole oscillations are associated with the electric-dipole ones.

On the other hand, the acoustic electro-magnetic mode of the trilayer system is characterized by the Drude weight

$$D_- = \lim_{\omega \rightarrow 0} \{\omega \text{Im}(\alpha_-\sigma_-)\}. \quad (17)$$

This mode does not usually couple to light because of the vanishing electric-dipole moment. However, in this case there is an effective electric-dipole moment as the current density of the outer layers is not exactly canceled by the current density of the middle layer. Moreover, this mode is again chiral, and will be accompanied by a magnetic component. We thus expect a rich and intricate plasmonic response in the mirror-symmetric, alternating twisted trilayer configuration.

Let us close the discussion on the collective modes by considering the two resonances for which  $|\varkappa|$  is large, defined in Eq. (14). For  $2(\sigma_0 + \sigma_1) \simeq \sigma_0^{12}$ , the in-phase Drude weight reduces to

$$D_+ \simeq \lim_{\omega \rightarrow 0} \{\omega \text{Im}(\sigma_0^{12})\}. \quad (18)$$

For  $\sigma_0 - \sigma_1 \simeq -2\sigma_0^{12}$ , the out-of-phase Drude weight becomes

$$D_- \simeq -2 \lim_{\omega \rightarrow 0} \{\omega \text{Im}(\sigma_0^{12})\}. \quad (19)$$

Both Drude weights,  $D_{\pm}$ , can directly be expressed by a Kubo formula for the effective twisted bilayer system; see Eq. (44) in Sec. III B.

### E. Irreducible representation

The symmetry group of the twisted bilayer system is  $D_3$ .<sup>49</sup> However, we now also have a mirror symmetry with respect to the middle layer, i.e.,  $D_{3h}$ . This property doubles the number of representations: we have four one-dimensional and two two-dimensional representations in total.

Due to the three-fold symmetry of the system, we can write each  $2 \times 2$  conductivity matrix as follows:

$$\sigma^{\ell\ell'} = \sigma_0^{\ell\ell'} \mathbf{1} + i\sigma_{xy}^{\ell\ell'} \tau_y. \quad (20)$$

Because of the mirror symmetry of the trilayer configuration, we only have four independent response functions, namely,  $\sigma_0^{11}$ ,  $\sigma_0^{12}$ ,  $\sigma_0^{13}$  and  $\sigma_0^{22}$ . These are related to the four one-dimensional representations of the group  $D_{3h}$ . Because of time reversal and mirror symmetry, we may further include the parameters  $\sigma_{xy}^{12}$  and  $\sigma_{xy}^{13}$ , which are related to the two two-dimensional representations of  $D_{3h}$ . Nonetheless, it turns out that  $\sigma_{xy}^{13} = 0$  in our alternating-twist setup, since the first and third layers ( $\ell = 1, 3$ ) have the same orientation.

### III. MICROSCOPIC THEORY FOR LAYER-RESOLVED CONDUCTIVITIES

In this section, we describe the conductivity parameters  $\sigma_{\nu\nu'}^{\ell\ell'}$  via the Kubo formulation. We highlight contributions from the effective twisted bilayer and single-layer systems, as well as a coupling between them and the effect of chirality. We show that the in-plane magnetic response of Sec. II B is negligible by invoking the moiré localization of the electronic Bloch wave functions at nearly flat bands. We also provide formulas for the Drude weights of Sec. II D. Our main assumptions are time reversal symmetry, isotropy, and mirror symmetry with respect to the middle layer.

#### A. Formalism

By Eq. (2), the surface conductivity matrix elements in the frequency domain are given by

$$\sigma_{\nu\nu'}^{\ell\ell'}(\omega) = \frac{e^2}{\hbar(\omega + i\delta)} \sum_{\{|\psi\rangle\}} f(E_\psi) \times \int_0^\infty dt e^{i(\omega+i\delta)t} \langle \psi | [j_\nu^\ell(t), j_{\nu'}^{\ell'}(0)] | \psi \rangle, \quad (21)$$

as  $\delta \downarrow 0$ , for real frequencies  $\omega$  ( $\ell, \ell' = 1, 2, 3$  and  $\nu, \nu' = x, y$ ). Here,  $|\psi\rangle$  is any normalized eigenvector of the trilayer Hamiltonian with eigenvalue  $E_\psi$ ; and  $f(E)$  is the Fermi-Dirac distribution. Regarding the  $K$ -valley, we use the Hamiltonian  $\mathcal{H}_K^{tr,i}$  of Appendix A;

and symmetrize the ensuing conductivity because of time reversal symmetry (Appendix B). In Eq. (21),  $j_\nu^\ell(t)$  has dimensions of inverse time, or frequency.

To describe the  $K$ -valley term  $\sigma_{\nu\nu',K}^{\ell\ell'}$ , we rewrite Eq. (21) by unitarily transforming each eigenvector  $|\psi\rangle$ , while  $\mathcal{H}_K^{tr,i}$  is transformed into the direct sum of the single-layer and effective twisted bilayer Hamiltonians  $\mathcal{H}_1$  and  $\mathcal{H}_2$ , respectively; see Eqs. (A14) and (A15) in Appendix A. The transformed eigenvectors of  $\mathcal{H}_K^{tr,i}$  are

$$|\underline{\psi}\rangle = \mathfrak{S}^\dagger |\psi\rangle = \begin{pmatrix} |b\rangle_1 \\ |b\rangle_2 \\ 0 \end{pmatrix} \quad \text{or} \quad \begin{pmatrix} 0 \\ 0 \\ |s\rangle \end{pmatrix}, \quad (22)$$

where  $(|b\rangle_1, |b\rangle_2)^T$  and  $|s\rangle$  denote any normalized-to-unity eigenvector of the effective bilayer Hamiltonian  $\mathcal{H}_2$  and monolayer Hamiltonian  $\mathcal{H}_1$ , respectively. Each of the indices  $b$  and  $s$  amounts to the combined band index and quasi-momentum of the moiré Brillouin zone, and  $\langle \mathbf{x} | \psi \rangle$  is composed of Bloch functions; cf. Eq. (44) below (Sec. III B). Note that

$$\mathcal{H}_2 \begin{pmatrix} |b\rangle_1 \\ |b\rangle_2 \end{pmatrix} = E_b \begin{pmatrix} |b\rangle_1 \\ |b\rangle_2 \end{pmatrix}, \quad \mathcal{H}_1 |s\rangle = E_s |s\rangle.$$

By slight abuse of notation,  $E_{b(s)}$  stands for the bilayer (single-layer) energy. Equation (21) becomes

$$\begin{aligned} \sigma_{\nu\nu',K}^{\ell\ell'}(\omega) &= \frac{e^2}{\hbar(\omega + i\delta)} \int_0^\infty dt e^{i(\omega+i\delta)t} \left\{ \sum_b f(E_b) \right. \\ &\quad \times \langle {}_1\langle b|, {}_2\langle b|, 0 \rangle [j_{\nu,K}^\ell(t), j_{\nu',K}^{\ell'}(0)] \begin{pmatrix} |b\rangle_1 \\ |b\rangle_2 \\ 0 \end{pmatrix} \\ &\quad + \sum_s f(E_s) \\ &\quad \left. \times \langle 0, 0, \langle s| \rangle [j_{\nu,K}^\ell(t), j_{\nu',K}^{\ell'}(0)] \begin{pmatrix} 0 \\ 0 \\ |s\rangle \end{pmatrix} \right\}, \quad (23) \end{aligned}$$

where  $j_{\nu,K}^\ell = \mathfrak{S}^\dagger j_{\nu,K}^\ell \mathfrak{S}$ . The symbol  $\sum_{b(s)}$  compactly expresses the combined summation over band indices and integration over the moiré Brillouin zone. The elements  $\langle \cdot | \cdot \rangle$  include integration in the spatial coordinates of the moiré cell. For details, see Appendix C.

#### B. Conductivities by mirror symmetry

Next, we focus on the mirror-symmetric setting, where the electron tunneling for layers 1, 2 is the same as that for layers 2, 3. In Appendix C, we discuss the more general setting without mirror symmetry by keeping the alternating twists, using  $\theta_{12} = -\theta_{23}$ .

Let  $\sigma_{BL}^{\zeta\zeta'}$  ( $\zeta, \zeta' = 1, 2$ ) and  $\sigma_{SL}$  denote the  $2 \times 2$  conductivity block matrices of the effective twisted bilayer

and single-layer systems that stem from our analysis. These parameters can be expressed in terms of matrix elements of pseudo-spin wave functions (Appendix C).

We first define  $\sigma_{BL}^{SS}$  and  $\sigma_{SL}$  phenomenologically, via a transformation of the layer-resolved surface current densities. Inspired by Eq. (22), we set

$$\begin{pmatrix} \tilde{\mathbf{J}}_1 \\ \tilde{\mathbf{J}}_2 \\ \tilde{\mathbf{J}}_3 \end{pmatrix} = \begin{pmatrix} \frac{1}{\sqrt{2}} & 0 & \frac{1}{\sqrt{2}} \\ 0 & 1 & 0 \\ \frac{1}{\sqrt{2}} & 0 & -\frac{1}{\sqrt{2}} \end{pmatrix} \begin{pmatrix} \mathbf{J}_1 \\ \mathbf{J}_2 \\ \mathbf{J}_3 \end{pmatrix}. \quad (24)$$

The electric fields are transformed by the same matrix into  $(\tilde{\mathbf{E}}_1, \tilde{\mathbf{E}}_2, \tilde{\mathbf{E}}_3)$ . The transformation for the current densities here follows directly from the conversion of the trilayer Hamiltonian into a direct sum of effective Hamiltonians (Appendix A). By the analysis in Appendix C, results of which we show below, the layer-resolved response implies a relation of the form

$$\begin{pmatrix} \tilde{\mathbf{J}}_1 \\ \tilde{\mathbf{J}}_2 \\ \tilde{\mathbf{J}}_3 \end{pmatrix} = \begin{pmatrix} \tilde{\sigma}^{11} & \tilde{\sigma}^{12} & 0 \\ \tilde{\sigma}^{21} & \tilde{\sigma}^{22} & 0 \\ 0 & 0 & \tilde{\sigma}_c \end{pmatrix} \begin{pmatrix} \tilde{\mathbf{E}}_1 \\ \tilde{\mathbf{E}}_2 \\ \tilde{\mathbf{E}}_3 \end{pmatrix}. \quad (25)$$

Given this response, the effective bilayer and monolayer conductivities are defined as

$$\sigma_{BL}^{11} = \sigma_{BL}^{22} = \tilde{\sigma}^{22}, \quad (26)$$

$$\sigma_{BL}^{12} = \sqrt{2}\tilde{\sigma}^{12}, \quad \sigma_{BL}^{21} = \sqrt{2}\tilde{\sigma}^{21} = (\sigma_{BL}^{12})^T, \quad (27)$$

$$\sigma_{SL} = 2\tilde{\sigma}^{11} - \tilde{\sigma}^{22}. \quad (28)$$

Thus, we can write  $\tilde{\sigma}^{11} = (\sigma_{BL}^{11} + \sigma_{SL})/2$ ,  $\tilde{\sigma}^{12} = \sigma_{BL}^{12}/\sqrt{2} = (\tilde{\sigma}^{12})^T$ , and  $\tilde{\sigma}^{22} = \sigma_{BL}^{11}$ . The effective-conductivity matrices have the forms

$$\begin{aligned} \sigma_{SL} &= \begin{pmatrix} \sigma_e^{(1)} & 0 \\ 0 & \sigma_e^{(1)} \end{pmatrix}, \\ \sigma_{BL}^{SS} &= \begin{pmatrix} \sigma_e^{(2)} & 0 \\ 0 & \sigma_e^{(2)} \end{pmatrix} \quad (\varsigma = 1, 2), \\ \sigma_{BL}^{12} &= \begin{pmatrix} \sigma_{e,xy}^{12} & \sigma_{e,xy}^{12} \\ -\sigma_{e,xy}^{12} & \sigma_{e,xy}^{12} \end{pmatrix} = (\sigma_{BL}^{21})^T, \end{aligned}$$

where  $\sigma_e^{(\varsigma)}$ ,  $\sigma_e^{12}$ , and  $\sigma_{e,xy}^{12}$  are scalar functions of  $\omega$  described below. The above matrix forms account for time reversal symmetry and isotropy (see Appendix C).

In addition, by Eq. (25) the surface current density  $\tilde{\mathbf{J}}_3 = (\mathbf{J}_1 - \mathbf{J}_3)/\sqrt{2}$  is proportional to the electric field  $\tilde{\mathbf{E}}_3 = (\mathbf{E}_1 - \mathbf{E}_3)/\sqrt{2}$  via  $\tilde{\sigma}_c$ . This matrix is diagonal and isotropic, and expresses a coupling between the two effective systems. For later convenience, we let

$$\tilde{\sigma}_c = \frac{1}{2}\sigma_c, \quad \sigma_c = \begin{pmatrix} \sigma_{0c} & 0 \\ 0 & \sigma_{0c} \end{pmatrix}. \quad (29)$$

The scalar  $\sigma_{0c}$  is discussed below.

By transforming Eq. (25) back to the layer-resolved response of Eq. (1), we identify the  $\sigma^{\ell\ell'}$  matrices as follows ( $\ell, \ell' = 1, 2, 3$ ):

$$\sigma^{11} = \sigma^{33} = \frac{1}{4}(\sigma_{BL}^{11} + \sigma_{SL} + \sigma_c), \quad (30)$$

$$\sigma^{12} = \frac{1}{2}\sigma_{BL}^{12} = (\sigma^{21})^T, \quad (31)$$

$$\sigma^{13} = \sigma^{31} = \frac{1}{4}(\sigma_{BL}^{11} + \sigma_{SL} - \sigma_c), \quad (32)$$

$$\sigma^{22} = \sigma_{BL}^{22}, \quad (33)$$

$$\sigma^{23} = \frac{1}{2}\sigma_{BL}^{21} = \sigma^{21} = (\sigma^{32})^T. \quad (34)$$

Notably, the mixing term  $\sigma_c = 2\tilde{\sigma}_c$  affects only  $\sigma^{11}$ ,  $\sigma^{13}$ ,  $\sigma^{31}$  and  $\sigma^{33}$ . Recalling the scalar parameters  $\sigma_0^{\ell\ell'}$  and  $\sigma_{xy}^{12}$  of Sec. II A, we obtain the formulas

$$\sigma_0^{11} = \frac{1}{4}(\sigma_e^{(1)} + \sigma_e^{(2)} + \sigma_{0c}), \quad (35)$$

$$\sigma_0^{12} = \frac{1}{2}\sigma_e^{12}, \quad \sigma_{xy}^{12} = \frac{1}{2}\sigma_{e,xy}^{12}, \quad (36)$$

$$\sigma_0^{13} = \frac{1}{4}(\sigma_e^{(1)} + \sigma_e^{(2)} - \sigma_{0c}), \quad (37)$$

$$\sigma_0^{22} = \sigma_e^{(2)}. \quad (38)$$

Hence, the optical responses in Secs. IIB and IIC can be expressed in terms of  $\sigma_e^{(1,2)}$ ,  $\sigma_{e,(xy)}^{12}$  and  $\sigma_{0c}$ , which pertain to the effective bilayer and single-layer systems.

Next, we describe the parameters of  $\sigma_{BL}^{SS}$ ,  $\sigma_{SL}$  and  $\sigma_c$  via inner products of pseudo-spin wave functions. For notational convenience, let  $\tau_{\pm} = \frac{1}{2}(\tau_x \pm i\tau_y)$  where  $\tau_{x,y}$  are the  $x, y$ -components of the Pauli matrices.

First, the matrix  $\sigma_c(\omega)$  emerges from the overlap of Bloch eigenvectors of the two effective systems in the Kubo trace formula. By  $\sigma_c = \text{diag}(\sigma_{0c}, \sigma_{0c})$ , we derive

$$\begin{aligned} \sigma_{0c} &= -i2g_v g_s \frac{v_F^2}{A_m} \frac{e^2}{\hbar(\omega + i\delta)} \sum_{bs} \frac{(f_b - f_s)\omega_{bs}}{(\omega + i\delta)^2 - \omega_{bs}^2} \\ &\quad \times (|{}_1\langle b|\tau_+|s\rangle|^2 + |{}_1\langle b|\tau_-|s\rangle|^2), \quad \delta \downarrow 0, \quad (39) \end{aligned}$$

where  $\omega_{bs} = (E_b - E_s)/\hbar$ ,  $f_{b(s)} = f(E_{b(s)})$ ,  $g_v$  ( $g_s$ ) is the valley (spin) degeneracy factor,  $v_F$  is the Fermi velocity of monolayer graphene, and  $A_m$  is the area of the reference moiré cell. This expression is simplified in view of  $|{}_1\langle b|\tau_+|s\rangle|^2 = |{}_1\langle b|\tau_-|s\rangle|^2$ , because of a symmetry of the effective Hamiltonians  $\mathcal{H}_{1,2}$  under the interchange of the sublattice indices. The relative magnitude of  $\sigma_{0c}$  is estimated in Sec. III C.

Another salient element is the chirality parameter,  $\sigma_{xy}^{12}$ , from the effective bilayer system. This equals

$$\begin{aligned} \sigma_{xy}^{12}(\omega) &= \frac{1}{2}\sigma_{e,xy}^{12} = ig_v g_s \frac{v_F^2}{A_m} \frac{e^2}{\hbar(\omega + i\delta)} \sum_{bb'} (f_b - f_{b'}) \\ &\quad \times \frac{\omega_{bb'} \text{Im}\{e^{-i\theta} ({}_2\langle b'|\tau_-|b\rangle_2) ({}_1\langle b|\tau_+|b'\rangle_1)\}}{(\omega + i\delta)^2 - \omega_{bb'}^2} \quad (40) \end{aligned}$$

where  $\omega_{bb'} = (E_b - E_{b'})/\hbar$ . For  $\theta = 0$ , this  $\sigma_{xy}^{12}$  vanishes, as expected. This property is derived by noting that for  $\theta = 0$  we have  ${}_1\langle b|\tau_{\pm}|b'\rangle_1 = {}_2\langle b|\tau_{\pm}|b'\rangle_2$ , switching layers in  $\mathcal{H}_2$ , where  ${}_1\langle b|\tau_{\pm}|b'\rangle_{1(2)} = ({}_{1(2)}\langle b'|\tau_{\mp}|b\rangle_{1(2)})^*$ . More generally, we have  $\sigma_{xy}^{12}(\omega; \theta) = -\sigma_{xy}^{12}(\omega; -\theta)$ .

The remaining response parameters are given by

$$\sigma_e^{(1)} = -i2g_v g_s \frac{v_F^2}{A_m} \frac{e^2}{\hbar(\omega + i\delta)} \sum_{ss'} \frac{(f_s - f_{s'})\omega_{ss'}}{(\omega + i\delta)^2 - \omega_{ss'}^2} \times |{}_s\langle \tau_+ | s' \rangle|^2, \quad (41)$$

$$\sigma_e^{(2)} = -ig_v g_s \frac{v_F^2}{A_m} \frac{e^2}{\hbar(\omega + i\delta)} \sum_{bb'} \frac{(f_b - f_{b'})\omega_{bb'}}{(\omega + i\delta)^2 - \omega_{bb'}^2} \times (|{}_1\langle b|\tau_+|b'\rangle_1|^2 + |{}_2\langle b'|\tau_-|b\rangle_2|^2), \quad (42)$$

$$\sigma_e^{12} = -i2g_v g_s \frac{v_F^2}{A_m} \frac{e^2}{\hbar(\omega + i\delta)} \sum_{bb'} \frac{(f_b - f_{b'})\omega_{bb'}}{(\omega + i\delta)^2 - \omega_{bb'}^2} \times \text{Re}\{e^{-i\theta} ({}_1\langle b|\tau_+|b'\rangle_1) ({}_2\langle b'|\tau_-|b\rangle_2)\}. \quad (43)$$

By Eqs. (42) and (43), regarding the effective bilayer system, we can show that  $\sigma_e^\eta(\omega; \theta) = \sigma_e^\eta(\omega; -\theta)$ .

We can now express parameters of Sec. II in terms of the above Kubo formulas. In particular, consider the Drude weights  $D_{\pm}$  (Sec. IID). For  $2(\sigma_0 + \sigma_1) \simeq \sigma_0^{12}$ , by Eqs. (18) and (43) we obtain

$$\frac{D_+}{D_0} \simeq \frac{9g_s g_v}{16\pi^2} t_G a_C^2 \int d\mathbf{k} \sum_{n,n'} \frac{f(E_{\mathbf{k},n}) - f(E_{\mathbf{k},n'})}{E_{\mathbf{k},n} - E_{\mathbf{k},n'}} \times \text{Re}\{e^{-i\theta} ({}_1\langle \mathbf{k}, n|\tau_+|\mathbf{k}, n'\rangle_1) ({}_2\langle \mathbf{k}, n'|\tau_-|\mathbf{k}, n\rangle_2)\}, \quad (44)$$

by using  $\hbar v_F = \frac{3}{2} a_C t_G$  and  $D_0 = t_G \frac{e^2}{\hbar^2}$ . In the above,  $t_G$  is the hopping energy in monolayer graphene,  $a_C$  is the carbon-carbon distance,  $|b\rangle = |\mathbf{k}, n\rangle$  denotes the Bloch eigenstate of the effective bilayer system with quasi-momentum  $\mathbf{k}$  at band  $n$ , and  $E_{\mathbf{k},n}$  is its energy. Integration is carried out over the moiré Brillouin zone. Note that, if  $\sigma_0 - \sigma_1 \simeq -2\sigma_0$ , by Eq. (19) the ratio  $\frac{D_-}{D_0}$  comes from multiplication of Eq. (44) by  $-2$ .

### C. In-plane magnetic response near magic angle

Next, we show that the in-plane magnetic response of Sec. IIB is negligible near charge neutrality for alternating twists close to the magic angle. By Eqs. (8), (35) and (37), this response reads

$$\mathbf{m}_{\parallel} = i\omega \frac{a^2}{4} \sigma_{0c}(\omega) \mathbf{B}_{\parallel} = \chi_m^c(\omega) \mathbf{B}_{\parallel}. \quad (45)$$

We need to estimate the coupling term  $\sigma_{0c}$ , or response  $\chi_m^c$ . We employ a localization ansatz for the electronic

Bloch wave functions of the effective twisted bilayer system at nearly flat bands, in the spirit of Ref. 50.

Consider the eigenstates of Eq. (22). For the effective bilayer system, our localization hypothesis reads<sup>50</sup>

$$\begin{pmatrix} \langle \mathbf{x}|b\rangle_1 \\ \langle \mathbf{x}|b\rangle_2 \end{pmatrix} \simeq e^{i(\mathbf{K}+\mathbf{k})\cdot\mathbf{x}} \Phi_n(\sqrt{\xi}\mathbf{x}/L_m) \begin{pmatrix} P_{1,n} \\ P_{2,n} \end{pmatrix} \quad (46)$$

near the  $K$  point. Here,  $P_{\ell,n}$  is a  $2 \times 1$  vector for the sublattice polarization in each layer ( $\ell = 1, 2$ ),  $n$  is the band index (e.g.,  $n = \pm 1$  for flat bands),  $L_m$  is the moiré length ( $|\mathbf{K}|L_m \gg 1$ ),  $\mathbf{k}$  is the quasi-momentum vector ( $k = |\mathbf{k}| \ll |\mathbf{K}|$ ), and  $\xi \simeq 3$ .<sup>50</sup> The function  $\Phi_n$  is localized in the moiré cell. By normalizing formula (46) with  $|P_{1,n}| \sim |P_{2,n}|$  we obtain

$$P_{\ell,n} \sim e^{i\vartheta_{\ell,n}} \sqrt{\frac{\xi}{4L_m^2}} (1, 1)^T, \quad (47)$$

where  $\vartheta_{\ell,n}$  is a phase that does not affect our results, and  $\Phi_n$  is normalized to unity. The symbol  $\sim$  means that numerical factors roughly equal to unity or smaller are ignored for the sake of order-of-magnitude estimates. The eigenvectors of the single-layer system are

$$\langle \mathbf{x}|s\rangle = \frac{1}{\sqrt{2A_m}} e^{i(\mathbf{K}+\mathbf{k})\cdot\mathbf{x}} \begin{pmatrix} 1 \\ \pm e^{i\theta/2} \frac{k_x + ik_y}{k} \end{pmatrix} \quad (48)$$

for its two bands, where  $A_m \sim L_m^2$ .

Let us invoke Eqs. (46) and (48) in Eq. (39). We assume that  $\omega < v_F k_m$  with  $k_m = \frac{2\pi}{L_m}$ . By only considering the nearly flat bands for the effective bilayer system, and relatively large energies of the effective monolayer system so that  $\omega_b - \omega_s \simeq -\omega_s$ , we have

$$\chi_m^c \sim \frac{g_v g_s}{2(4\pi)^2} v_F^2 a^2 \frac{e^2}{\hbar} \int d\mathbf{k} \sum_{n_b, n_s = \pm 1} |\bar{C}_{n_b}(\xi)|^2 \times [f(E_{\mathbf{k},n_b}) - f(E_{\mathbf{k},n_s})] \frac{n_s v_F k}{(v_F k)^2 - (\omega + i\delta)^2}$$

as  $\delta \downarrow 0$ . In the above,  $E_{\mathbf{k},n_b}$  ( $E_{\mathbf{k},n_s}$ ) is the energy of the effective bilayer (single-layer) system at band  $n_b$  ( $n_s$ ), and

$$\bar{C}_n(\xi) = \frac{1}{\sqrt{\xi}} \int d\mathbf{x}' \Phi_n(\mathbf{x}') \quad (n = \pm 1)$$

over the transformed moiré cell by  $\mathbf{x} \mapsto \mathbf{x}' = \frac{\sqrt{\xi}}{L_m} \mathbf{x}$ . The scaling of this integral with  $\sqrt{\xi}$  ensures that  $|\bar{C}_n| \lesssim 1$  regardless of the value of  $\xi > 0$ . We evaluate the integral for  $\chi_m^c$  by neglecting terms proportional to or smaller than  $\frac{\omega}{v_F k_m} \ln(\frac{v_F k_m}{\omega})$ ; thus,  $\hbar\omega$  may not exceed a few hundred meV which poses no practical restriction.

To show that  $\chi_m^c$  is negligibly small, we compare it to  $\chi_0 = \hbar^{-2} e^2 t_G a_C^2$ , which is used in discussions about lattice effects on the out-of-plane magnetic susceptibility in the single-layer graphene.<sup>51</sup> Hence, we compute

$$\frac{\chi_m^c}{\chi_0} \sim \frac{3}{8} g_v g_s \langle Df \rangle_m \frac{a^2/a_C}{L_m} \simeq 1.2 \langle f \rangle_m^c \quad (49)$$

with  $a = 1 \text{ nm} \simeq 7a_C$ ,  $L_m = a_C \sqrt{3\sqrt{3i^2 + 3i + 1}} \simeq 61.43a_C$  for  $i = 20$ , regarding the trilayer configuration (Fig. 1). Notice the linear scaling of  $\frac{\chi_m^c}{\chi_0^c}$  with the inverse moiré length. The positive factor  $\langle f \rangle_m^c$  depends on the  $|\bar{C}_n|^c$ 's of nearly flat bands and the Fermi-Dirac distribution,  $f$ ; and expresses a weighted radial-momentum average of  $f(E_-(k)) - f(E_+(k))$  for the monolayer system energies  $E_\pm(k) = \pm \hbar v_F k$ , from  $E_{\mathbf{k}, n_s}$  with  $n_s = \pm 1$ . This average is defined by

$$\langle f \rangle_m^c = \frac{1}{2} (|\bar{C}_1|^2 + |\bar{C}_{-1}|^2) \times \left\{ \frac{1}{k_m} \int_0^{k_m} dk [f(E_-(k)) - f(E_+(k))] \right\}.$$

We see that  $\langle f \rangle_m^c < 1$ .

Formula (49) suggests that the in-plane magnetic response of the twisted trilayer is very weak, since it is comparable to or smaller than the corresponding atomistic (lattice) effect in monolayer graphene. Evidently, the response function  $\chi_m^c(\omega)$  has a plateau in frequency for  $\omega \lesssim v_F k_m$ . The extension of our analysis to higher bands of the effective bilayer system might be pursued with a similar localization ansatz.<sup>52</sup>

#### D. Estimates for effective magnetic response and Drude weights

Next, by scaling arguments we discuss the effective magnetic response  $\chi_m$  and chirality  $\sigma_{xy}^{12}$  (Sec. II C), and Drude weights  $D_\pm$  (Sec. II D). We indicate how these quantities scale with the moiré length,  $L_m$ , by virtue of a localization ansatz for the Bloch wave functions near the magic angle of the trilayer configuration which is assumed to persist also with doping.<sup>52</sup>

To simplify the analysis for  $\chi_m$  and  $D_\pm$ , consider large  $|\varkappa|$  by Eq. (14). This occurs if  $\sigma_0 - \sigma_1 \simeq -2\sigma_0^{12}$  or  $2(\sigma_0 + \sigma_1) \simeq \sigma_0^{12}$ . In the former case, the formula for  $\chi_m$  is simplified to  $\chi_m \simeq -i\omega a^2 \sigma_0^{12} = -\frac{1}{2} i\omega a^2 \sigma_e^{12}$ . By Eq. (43) and the procedure of Sec. III C, we find

$$\left| \frac{\chi_m}{\chi_0} \right| \sim \frac{3}{32} g_v g_s \langle f \rangle_m \frac{a^2/a_C}{L_m} \frac{v_F}{v_{F*}} \sim 0.3 \langle f \rangle_m \frac{v_F}{v_{F*}}. \quad (50)$$

Here,  $v_{F*}$  is the Fermi velocity of the effective twisted bilayer system, and  $\langle f \rangle_m$  is the positive average

$$\langle f \rangle_m = \frac{1}{k_m} \int_0^{k_m} dk \{ f(E_{-1}^b(k)) - f(E_1^b(k)) \},$$

where  $E_{\pm 1}^b(k)$  come from the flat-band energies,  $E_{\mathbf{k}, n_b}$  with  $n_b = \pm 1$ , of the effective bilayer system. Note that Eq. (50) should hold if  $\frac{\omega}{v_{F*} k_m}$  is small. Because of the kinematic factor  $\frac{v_F}{v_{F*}}$  in the expression for  $|\frac{\chi_m}{\chi_0}|$ , the effective magnetic response  $\chi_m$  is much larger than  $\chi_m^c$  and measurable. The frequency plateau for  $\chi_m^c(\omega)$  (Sec. III C) is decreased by  $\frac{v_{F*}}{v_F}$  in the case of  $\chi_m(\omega)$ .

We can now apply similar approximations to the Drude weights by formulas (18) and (19). For example, by Eq. (18), which holds if  $2(\sigma_0 + \sigma_1) \simeq \sigma_0^{12}$ , we obtain

$$\frac{D_+}{D_0} \sim \frac{3}{16} g_v g_s \langle f \rangle_m \frac{a_C}{L_m} \frac{v_F}{v_{F*}} \quad (51)$$

where we defined  $D_0 = t_G e^2 / \hbar^2$ . A similar estimate can be found for  $D_-$  if  $\sigma_0 - \sigma_1 \simeq -2\sigma_0^{12}$ .

It remains to estimate the chirality,  $\sigma_{xy}^{12}$ , by use of Eq. (40); cf. Sec. II C for response function  $G = a\sigma_{xy}^{12}$ . Near charge neutrality, we find

$$\left| \frac{\text{Im}G}{G_0} \right| \sim \frac{3}{2} \langle f \rangle_m \frac{t_G}{\hbar\omega} \frac{a}{L_m} \frac{v_F}{v_{F*}}, \quad (52a)$$

$$\left| \frac{\text{Re}G}{G_0} \right| \sim \frac{3}{4} \langle f \rangle_m \frac{t_G}{\hbar v_F q_m} \frac{a}{L_m} \left( \frac{v_F}{v_{F*}} \right)^2, \quad (52b)$$

where  $G_0 = a_C \sigma_G = a_C e^2 / (4\hbar)$ .

Similar scaling relations for  $\frac{v_F}{v_{F*}} \gg 1$  are obtained for the twisted bilayer graphene in Ref. 49. The predicted Condon instability for the twisted bilayer graphene at charge neutrality would thus also persist in twisted trilayer graphene. However, this would occur at finite doping that matches the two resonant conditions for  $|\varkappa| \gg 1$ .

## IV. CONCLUSION

In this paper, we analytically described the overall optical response of the alternating-twist trilayer system. First, we studied implications of symmetry principles, making assumptions about the trilayer conductivity tensor under mirror symmetry with respect to the middle layer. We argued that the emergent optical response is composed of: (i) an effective electro-magnetic response akin to the twisted-bilayer graphene constitutive relations, where chirality plays a key role; and (ii) an in-plane magnetic response. We made predictions for the character of the bulk plasmonic modes in this trilayer configuration. Second, by invoking microscopic principles via the Kubo formulation, we showed that the magnetic response is proportional to a coupling between effective twisted bilayer and monolayer systems. We estimated that the magnetic response is very weak, because of the dramatic effect of the moiré scale near the magic angle. This estimate can explain the practical absence of an in-plane magnetic susceptibility in the alternating twisted trilayer graphene.

The results in this paper motivate further studies in the optical response of twisted multilayer systems. In fact, a naive scaling argument indicates that the magnetic response should increase monotonically with the number of layers. A detailed study of this behavior can be the subject of future work.



## ACKNOWLEDGMENTS

The authors thank E. Kaxiras, M. Luskin, J. T. Waters and Z. Zhu for discussions. The work of T.S. was supported by grant PID2020-113164GBI00 funded by MCIN/AEI/10.13039/501100011033, PID2023-146461NB-I00 funded by Ministerio de Ciencia, Innovación y Universidades as well as by the CSIC Research Platform on Quantum Technologies PTI-001.

### Appendix A: Hamiltonian of trilayer system and unitary transformation to direct sum

In this appendix, we describe the Dirac Hamiltonian of the alternating-twist trilayer system in real space; and transform it unitarily into a direct sum of effective twisted bilayer and single-layer Hamiltonians, following Ref. 45. Our setting lacks mirror symmetry.

#### 1. Model Hamiltonian and moiré potentials

The electron Schrödinger state vector is of the form

$$\psi = (\{\psi_\ell^s\})^T = (\psi_1^A \ \psi_1^B \ \psi_2^A \ \psi_2^B \ \psi_3^A \ \psi_3^B)^T.$$

The twist angle of layer  $\ell$  is  $\theta_\ell = (-1)^\ell \theta/2$  ( $\ell = 1, 2, 3$ ). In the sublattice-layer representation, the unperturbed Hamiltonian of the  $K$  valley reads

$$\mathcal{H}_K^{tri} = \begin{pmatrix} \mathfrak{D}(\theta) & \mathfrak{T}^{12}(\mathbf{x}) & 0 \\ \mathfrak{T}^{12}(\mathbf{x})^\dagger & \mathfrak{D}(-\theta) & \mathfrak{T}^{23}(\mathbf{x}) \\ 0 & \mathfrak{T}^{23}(\mathbf{x})^\dagger & \mathfrak{D}(\theta) \end{pmatrix}; \quad (\text{A1})$$

$\mathbf{x} = (x, y)^T$  is the position vector in the reference plane ( $\mathbf{x} \in \mathbb{R}^2$ ). The matrix-valued Dirac operator is

$$\mathfrak{D}(\theta) = v_F \hbar \begin{pmatrix} 0 & -2ie^{-i\frac{\theta}{2}} \partial \\ -2ie^{i\frac{\theta}{2}} \bar{\partial} & 0 \end{pmatrix}, \quad (\text{A2})$$

where  $v_F \simeq 10^6$  m/s is the Fermi velocity of graphene,  $\partial = (\partial_x - i\partial_y)/2$  and  $\bar{\partial} = (\partial_x + i\partial_y)/2$  in the  $xy$  plane.

The related moiré potentials are described by

$$\mathfrak{T}^{\ell\ell'}(\mathbf{x}) = \begin{pmatrix} w_{AA}^{\ell\ell'} U_0^{\ell\ell'}(\mathbf{x}) & w_{AB}^{\ell\ell'} U_1^{\ell\ell'}(\mathbf{x}) \\ w_{AB}^{\ell\ell'} U_1^{\ell\ell'*}(-\mathbf{x}) & w_{AA}^{\ell\ell'} U_0^{\ell\ell'}(\mathbf{x}) \end{pmatrix} \quad (\text{A3})$$

for  $\ell' = \ell + 1$  (if  $\ell = 1, 2$ ), where  $w_{AA}^{\ell\ell'} = \kappa w_{AB}^{\ell\ell'}$ ,  $\kappa > 0$ , the coefficients  $w_{AB}^{\ell\ell'}$  have units of energy and express interlayer tunneling, and

$$U_\xi^{\ell\ell'}(\mathbf{x}) = \sum_{n=1}^3 e^{-i\xi(n-1)\phi} e^{-i\mathbf{q}_n^{\ell\ell'} \cdot (\mathbf{x} - \mathbf{D}_{\ell\ell'})} \quad (\text{A4})$$

with  $\phi = 2\pi/3$  and  $\xi = 0, 1$ . Here, we define<sup>45</sup>

$$\mathbf{q}_1^{\ell\ell'} = 2k_D \sin\left(\frac{\theta_{\ell'\ell}}{2}\right) \mathcal{R}_{\phi_{\ell\ell'}} \cdot (0, -1)^T, \quad (\text{A5})$$

$$\mathbf{q}_{2,3}^{\ell\ell'} = \mathcal{R}_{\pm\phi} \cdot \mathbf{q}_1^{\ell\ell'}, \quad (\text{A6})$$

$$\mathbf{D}_{\ell\ell'} = \frac{\mathbf{d}_\ell + \mathbf{d}_{\ell'}}{2} + i \cot\left(\frac{\theta_{\ell'\ell}}{2}\right) \tau_y \cdot \frac{\mathbf{d}_\ell - \mathbf{d}_{\ell'}}{2}, \quad (\text{A7})$$

$$\theta_{\ell'\ell} = \theta_{\ell'} - \theta_\ell, \quad \phi_{\ell\ell'} = \frac{\theta_\ell + \theta_{\ell'}}{2}, \quad (\text{A8})$$

$$\mathcal{R}_\phi = \begin{pmatrix} \cos \phi & -\sin \phi \\ \sin \phi & \cos \phi \end{pmatrix},$$

where  $k_D = |\mathbf{K}| = \frac{4\pi}{3\sqrt{3}a_C}$  is the Dirac momentum,  $\tau_y$  is the  $y$ -Pauli matrix, and  $a_C \simeq 1.42$  Å is the carbon-carbon distance. The vector  $\mathbf{d}_\ell$  is the lateral shift of the  $\ell$ -th layer; and  $\mathbf{D}_{\ell\ell'}$  amounts to shifts in the potentials. We set  $\mathbf{d}_\ell = \mathbf{d} = (d_1, d_2)^T$  for all  $\ell$  by which  $\mathbf{D}_{\ell\ell'} = \mathbf{d}$ .

Next, we non-dimensionalize the model via the mapping  $\mathbf{x} \mapsto \check{\mathbf{x}} = 2k_D \sin(\theta/2) \mathbf{x}$ .<sup>45</sup> Let the scaled position and shift vectors be  $\check{\mathbf{x}}$  and  $\check{\mathbf{d}}$ . The Hamiltonian  $\mathcal{H}_K^{tri}$  exhibits the energy scale  $2v_F \hbar k_D \sin(\theta/2)$ ;  $\mathcal{H}_K^{tri} \mapsto \check{\mathcal{H}}_K^{tri} = (2v_F \hbar k_D \sin(\theta/2))^{-1} \mathcal{H}_K^{tri}$ . We define

$$\alpha_{\ell\ell'} = \frac{w_{AB}^{\ell\ell'}}{2v_F \hbar k_D \sin(\theta/2)} > 0, \quad \ell' = \ell + 1 \ (\ell = 1, 2).$$

For ease of notation, we remove the breve symbol from  $\check{\mathbf{x}}, \check{\mathbf{d}}$  and  $\check{\mathcal{H}}_K^{tri}$ , thus using  $\mathbf{x}, \mathbf{d} = (d_1, d_2)^T$  and  $\mathcal{H}_K^{tri}$  as the moiré-scaled variables; ditto for the potentials  $\mathfrak{T}^{\ell\ell'}$ .

Hence, we now have the dimensionless potentials

$$\mathfrak{T}^{12}(\mathbf{x}) = \begin{pmatrix} \kappa \alpha_{12} U_0(\mathbf{x}) & \alpha_{12} U_1^*(-\mathbf{x}) \\ \alpha_{12} U_1(\mathbf{x}) & \kappa \alpha_{12} U_0(\mathbf{x}) \end{pmatrix},$$

$$\mathfrak{T}^{23}(\mathbf{x}) \simeq \begin{pmatrix} \kappa \alpha_{23} U_0^*(\mathbf{x}) & \alpha_{23} U_1^*(\mathbf{x}) \\ \alpha_{23} U_1(-\mathbf{x}) & \kappa \alpha_{23} U_0^*(\mathbf{x}) \end{pmatrix}.$$

If  $\alpha_{12} \neq \alpha_{23}$  the ensuing Hamiltonian may lack mirror symmetry. This symmetry is recovered if  $\alpha_{12} = \alpha_{23}$ .

In view of  $|\mathbf{d}| \ll 1$ , we have set

$$\begin{aligned} U_0(\mathbf{x}) &= U_0^{12}(\mathbf{x}), & U_0^{12*}(\mathbf{x}) &= U_0^*(\mathbf{x}), \\ U_0^{23}(\mathbf{x}) &= U_0^*(\mathbf{x}), & U_0^{23*}(\mathbf{x}) &= U_0(\mathbf{x}), \\ U_1(\mathbf{x}) &= U_1^{12*}(-\mathbf{x}), & U_1^{12}(\mathbf{x}) &= U_1^*(-\mathbf{x}), \\ U_1^{23}(\mathbf{x}) &\simeq U_1^*(\mathbf{x}), & U_1^{23*}(-\mathbf{x}) &\simeq U_1(-\mathbf{x}). \end{aligned}$$

In the above, the first and fifth equations introduce  $U_0$  and  $U_1$ , while the last two equations are implied by the condition  $|\mathbf{d}| \ll 1$ .

For the sake of clarity, we give the explicit formulas

for  $U_0$  and  $U_1$  at the moiré scale. These are

$$\begin{aligned} U_0(\mathbf{x}) &= e^{i(y-d_2)} + e^{-i(\frac{\sqrt{3}}{2}(x-d_1)+\frac{1}{2}(y-d_2))} \\ &\quad + e^{-i(-\frac{\sqrt{3}}{2}(x-d_1)+\frac{1}{2}(y-d_2))} \\ &\simeq e^{iy} + e^{-i(\frac{\sqrt{3}}{2}x+\frac{1}{2}y)} + e^{-i(-\frac{\sqrt{3}}{2}x+\frac{1}{2}y)}, \end{aligned} \quad (\text{A9})$$

$$\begin{aligned} U_1(\mathbf{x}) &\simeq e^{iy} + e^{i\frac{2\pi}{3}} e^{-i(\frac{\sqrt{3}}{2}x+\frac{1}{2}y)} \\ &\quad + e^{-i\frac{2\pi}{3}} e^{-i(-\frac{\sqrt{3}}{2}x+\frac{1}{2}y)}. \end{aligned} \quad (\text{A10})$$

The Hamiltonian  $\mathcal{H}_{K'}^{tri}$  of the  $K'$  valley comes from the complex conjugation of  $\mathcal{H}_K^{tri}$  above. Thus, we write

$$\mathcal{H}_{K'}^{tri} = (\mathcal{H}_K^{tri})^*,$$

in real space. Thus, the eigenvector (basis) sets of the two Hamiltonians are related by an anti-unitary transformation. The total contribution to the conductivity from both valleys under time reversal symmetry in linear response can be extracted from the  $K$ -valley Hamiltonian by a simple transposition. One must then symmetrize the optical conductivity; see Appendix B.

## 2. Unitary transformations and direct sum

Next, we outline the steps of a unitary transformation on  $\mathcal{H}_K^{tri}$ , which eventually yields the mapping

$$\mathcal{H}_K^{tri} \mapsto \mathcal{H}_K^{eff} = \mathfrak{S}^\dagger \mathcal{H}_K^{tri} \mathfrak{S} = \mathcal{H}_{\lambda,K}^{(2)} \oplus \mathcal{H}_K^{(1)}, \quad (\text{A11})$$

where  $\mathcal{H}_{\lambda,K}^{(2)}$  is the effective,  $K$ -valley twisted bilayer Hamiltonian with parameter  $\lambda = \sqrt{\alpha_{12}^2 + \alpha_{23}^2}$ , and  $\mathcal{H}_K^{(1)}$  is the respective single-layer Hamiltonian, as explained below. Hence, we can write any eigenvector of  $\mathcal{H}_K^{eff}$  in the form  $(|b\rangle_1, |b\rangle_2, 0)^T$  or  $(0, 0, |s\rangle)^T$  where  $(|b\rangle_1, |b\rangle_2)^T$  and  $|s\rangle$  are eigenvectors of  $\mathcal{H}_{\lambda,K}^{(2)}$  and  $\mathcal{H}_K^{(1)}$ , respectively. We have

$$\mathcal{H}_{\lambda,K}^{(2)} \begin{pmatrix} |b\rangle_1 \\ |b\rangle_2 \end{pmatrix} = E_b^{(2)} \begin{pmatrix} |b\rangle_1 \\ |b\rangle_2 \end{pmatrix}, \quad \mathcal{H}_K^{(1)} |s\rangle = E_s^{(1)} |s\rangle;$$

$E_{b,s}^{(2,1)}$  is the eigenvalue of the Dirac Hamiltonian for the twisted bilayer ( $b$ ) and single-layer ( $s$ ) system. Each of the symbols  $s$  and  $b$  stands for the combined band index and continuum quasi-momentum variable of the scaled Brillouin zone. We set  $E_s = E_s^{(1)}$  and  $E_b = E_b^{(2)}$ .

We will show that in the sublattice-layer form<sup>45</sup>

$$\mathfrak{S} = \begin{pmatrix} \alpha_{12}/\lambda & 0 & \alpha_{23}/\lambda \\ 0 & 1 & 0 \\ \alpha_{23}/\lambda & 0 & -\alpha_{12}/\lambda \end{pmatrix}. \quad (\text{A12})$$

Note that  $\mathfrak{S}$  is represented by a  $6 \times 6$  matrix. In the case with mirror symmetry, if  $\alpha_{12} = \alpha_{23}$ , we have

$$\mathfrak{S} = \frac{1}{\sqrt{2}} \begin{pmatrix} 1 & 0 & 1 \\ 0 & \sqrt{2} & 0 \\ 1 & 0 & -1 \end{pmatrix}. \quad (\text{A13})$$

This unitary transformation is described as a result of four basic, successive unitary operations, as detailed below.<sup>45</sup> To simplify notation, we will omit the valley index ( $K$ ), unless we state otherwise.

### a. Layer ordering

We apply  $\mathcal{H}^{tri} \mapsto \overset{\circ}{\mathcal{H}} := \Omega^\dagger \mathcal{H}^{tri} \Omega$  with state vector

$$\begin{aligned} \psi &= (\psi_1^A \quad \psi_1^B \quad \psi_2^A \quad \psi_2^B \quad \psi_3^A \quad \psi_3^B)^T \\ \mapsto \overset{\circ}{\psi} &= \Omega^\dagger \psi = (\psi_1^A \quad \psi_2^A \quad \psi_3^A \quad \psi_1^B \quad \psi_2^B \quad \psi_3^B)^T. \end{aligned}$$

The transformation operator  $\Omega$  in matrix form is

$$\Omega = \begin{pmatrix} 1 & 0 & 0 & 0 & 0 & 0 \\ 0 & 0 & 0 & 1 & 0 & 0 \\ 0 & 1 & 0 & 0 & 0 & 0 \\ 0 & 0 & 0 & 0 & 1 & 0 \\ 0 & 0 & 1 & 0 & 0 & 0 \\ 0 & 0 & 0 & 0 & 0 & 1 \end{pmatrix}.$$

### b. Layer alignment

We now apply  $\overset{\circ}{\mathcal{H}} \mapsto \check{\mathcal{H}} = Y^\dagger \overset{\circ}{\mathcal{H}} Y$  so that

$$\begin{aligned} \overset{\circ}{\psi} &= (\psi_1^A \quad \psi_2^A \quad \psi_3^A \quad \psi_1^B \quad \psi_2^B \quad \psi_3^B)^T \\ \mapsto \check{\psi} &= Y^\dagger \overset{\circ}{\psi} = (\psi_1^A \quad \psi_3^A \quad \psi_2^A \quad \psi_1^B \quad \psi_3^B \quad \psi_2^B)^T \end{aligned}$$

where

$$Y = \begin{pmatrix} 1 & 0 & 0 & 0 & 0 & 0 \\ 0 & 0 & 1 & 0 & 0 & 0 \\ 0 & 1 & 0 & 0 & 0 & 0 \\ 0 & 0 & 0 & 1 & 0 & 0 \\ 0 & 0 & 0 & 0 & 0 & 1 \\ 0 & 0 & 0 & 0 & 1 & 0 \end{pmatrix}.$$

Thus, we have<sup>45</sup>

$$\check{\mathcal{H}} = \begin{pmatrix} \mathcal{M} & \mathcal{D}^\dagger \\ \mathcal{D} & \mathcal{M} \end{pmatrix},$$

$$\begin{aligned} \mathcal{M} &= \kappa \begin{pmatrix} 0 & 0 & \alpha_{12} U_0(\mathbf{x}) \\ 0 & 0 & \alpha_{23} U_0(\mathbf{x}) \\ \alpha_{12} U_0^*(\mathbf{x}) & \alpha_{23} U_0^*(\mathbf{x}) & 0 \end{pmatrix} \\ &= \kappa \begin{pmatrix} \mathbf{0} & W U_0(\mathbf{x}) \\ W^T U_0^*(\mathbf{x}) & 0 \end{pmatrix}, \quad W = \begin{pmatrix} \alpha_{12} \\ \alpha_{23} \end{pmatrix}. \end{aligned}$$

Here,  $\mathcal{D}$  is represented by the following  $3 \times 3$  matrix:

$$\mathcal{D} = \begin{pmatrix} -2ie^{i\theta/2}\bar{\partial} & W U_1(\mathbf{x}) \\ W^T U_1(-\mathbf{x}) & -2ie^{-i\theta/2}\bar{\partial} \end{pmatrix}.$$

c. *Singular-value decomposition*

Next, we apply  $\check{\mathcal{H}} \mapsto \widehat{\mathcal{H}} = V^\dagger \check{\mathcal{H}} V$  where

$$V = \begin{pmatrix} \mathcal{V} & 0 \\ 0 & \mathcal{V} \end{pmatrix}, \quad \mathcal{V} = \text{diag}(\mathcal{A}, \mathcal{B}),$$

and the  $2 \times 2$  matrix  $\mathcal{A}$  and scalar  $\mathcal{B}$  stem from  $W = \mathcal{A}\Lambda\mathcal{B}^*$  with  $\Lambda = (\lambda, 0)^T$  and  $\lambda = \sqrt{W^T W} = \sqrt{\alpha_{12}^2 + \alpha_{23}^2}$ . By a direct computation, we have

$$\mathcal{A} = \begin{pmatrix} \alpha_{12}/\lambda & \alpha_{23}/\lambda \\ \alpha_{23}/\lambda & -\alpha_{12}/\lambda \end{pmatrix}, \quad \mathcal{B} = 1.$$

The transformed Hamiltonian is thus written as

$$\widehat{\mathcal{H}} = \begin{pmatrix} 0 & 0 & \kappa\lambda U_0(\mathbf{x}) & -2ie^{-i\theta/2}\partial & 0 & \lambda U_1^*(-\mathbf{x}) \\ 0 & 0 & 0 & 0 & -2ie^{-i\theta/2}\partial & 0 \\ \kappa\lambda U_0^*(\mathbf{x}) & 0 & 0 & \lambda U_1^*(\mathbf{x}) & 0 & -2ie^{i\theta/2}\partial \\ -2ie^{i\theta/2}\bar{\partial} & 0 & \lambda U_1(\mathbf{x}) & 0 & 0 & \kappa\lambda U_0(\mathbf{x}) \\ 0 & -2ie^{i\theta/2}\bar{\partial} & 0 & 0 & 0 & 0 \\ \lambda U_1(-\mathbf{x}) & 0 & -2ie^{-i\theta/2}\bar{\partial} & \kappa\lambda U_0^*(\mathbf{x}) & 0 & 0 \end{pmatrix}.$$

d. *Conversion to direct sum*

We apply  $\widehat{\mathcal{H}} \mapsto \mathcal{H}^{eff} = Z^\dagger \widehat{\mathcal{H}} Z = \mathcal{H}_\lambda^{(2)} \oplus \mathcal{H}^{(1)}$  with

$$Z = \begin{pmatrix} 1 & 0 & 0 & 0 & 0 & 0 \\ 0 & 0 & 0 & 0 & 1 & 0 \\ 0 & 0 & 1 & 0 & 0 & 0 \\ 0 & 1 & 0 & 0 & 0 & 0 \\ 0 & 0 & 0 & 0 & 0 & 1 \\ 0 & 0 & 0 & 1 & 0 & 0 \end{pmatrix}.$$

In the above,  $\mathcal{H}^{(1)}$  and  $\mathcal{H}_\lambda^{(2)}$  denote the moiré-scaled effective single-layer and twisted bilayer Hamiltonians, respectively. To simplify notation, set  $\mathcal{H}^{(1)} = \mathcal{H}_1$  and  $\mathcal{H}_\lambda^{(2)} = \mathcal{H}_2$ . These operators read

$$\mathcal{H}_1 = \mathfrak{D}(\theta) = \begin{pmatrix} 0 & -2ie^{-i\theta/2}\partial \\ -2ie^{i\theta/2}\bar{\partial} & 0 \end{pmatrix} \quad (\text{A14})$$

and

$$\mathcal{H}_2 = \begin{pmatrix} \mathfrak{D}(\theta) & \lambda\mathcal{U}(\mathbf{x}) \\ \lambda\mathcal{U}(\mathbf{x})^\dagger & \mathfrak{D}(-\theta) \end{pmatrix}, \quad (\text{A15})$$

where

$$\mathcal{U}(\mathbf{x}) = \begin{pmatrix} \kappa U_0(\mathbf{x}) & U_1^*(-\mathbf{x}) \\ U_1(\mathbf{x}) & \kappa U_0(\mathbf{x}) \end{pmatrix}.$$

In summary, the operator  $\mathfrak{S}$  of Eq. (A12), which converts the  $K$ -valley Hamiltonian  $\mathcal{H}_K^{tr i}$  to  $\mathcal{H}_K^{eff}$ , is computed directly by  $\mathfrak{S} = \Omega Y V Z$ . The corresponding matrix is real. Hence, the same matrix is used to convert the  $K'$ -valley Hamiltonian,  $\mathcal{H}_{K'}^{tr i} = (\mathcal{H}_K^{tr i})^*$  in real space, into a direct sum of effective twisted bilayer and single-layer Hamiltonians.

## Appendix B: On time reversal symmetry

In this appendix, we discuss implications of time reversal symmetry for the surface conductivity. The total electronic Hamiltonian,  $\mathcal{H}$ , of the multi-layered system in real space thus satisfies  $\mathcal{H} = \mathcal{H}^*$ .

We show that a time reversal ( $\mathcal{T}$ -) symmetric  $\mathcal{H}$  implies a symmetric conductivity matrix, in the sense that interchanging the layer and polarization index pairs leaves the matrix invariant. In particular, we show that (for  $\nu, \nu' = x, y$  and  $\ell, \ell' = 1, 2, 3$ )

$$\sigma_{\nu\nu'}^{\ell\ell'}(\omega) = \sigma_{\nu'\nu}^{\ell'\ell}(\omega), \quad \text{every } \omega. \quad (\text{B1})$$

To prove Eq. (B1), we start with the fact that there exists an anti-unitary transformation,  $\mathfrak{U}$ , such that for each eigenvector  $|\psi\rangle$  of  $\mathcal{H}$  we have the invariance property  $|\psi\rangle = \mathfrak{U}|\psi\rangle$ . We apply  $\mathfrak{U}^{-1}j_{0\nu}^\ell\mathfrak{U} = -j_{0\nu}^\ell$ , where  $j_{0\nu}^\ell$  denotes the  $\nu$ -directed initial current of the  $l$ -th layer.

The trace of the Kubo formulation yields the following formula for the layer-resolved surface conductivity:

$$\begin{aligned} \sigma_{\nu\nu'}^{\ell\ell'}(\omega) &= -\frac{e^2}{\hbar(\omega + i0^+)} \sum_{\{|\psi\rangle, |\psi'\rangle\}} \frac{f(E_\psi) - f(E_{\psi'})}{i(\omega + i0^+ + \omega_{\psi\psi'})} \\ &\quad \times \langle \psi | \mathfrak{U}^{-1} j_{0,\nu}^\ell \mathfrak{U} | \psi' \rangle^* \langle \psi' | \mathfrak{U}^{-1} j_{0,\nu'}^{\ell'} \mathfrak{U} | \psi \rangle^* \\ &= -\frac{e^2}{\hbar(\omega + i0^+)} \sum_{\{|\psi\rangle, |\psi'\rangle\}} \frac{f(E_\psi) - f(E_{\psi'})}{i(\omega + i0^+ + \omega_{\psi\psi'})} \\ &\quad \times \langle \psi | (j_{0,\nu'}^{\ell'})^\dagger | \psi' \rangle \langle \psi' | (j_{0,\nu}^\ell)^\dagger | \psi \rangle \quad (\text{real } \omega). \end{aligned}$$

Here,  $E_\psi$  is the energy (eigenvalue of  $\mathcal{H}$ ) corresponding to the normalized eigenvector  $|\psi\rangle$  of  $\mathcal{H}$ ,  $f(E)$  is the Fermi-Dirac distribution, and  $\omega_{\psi\psi'} = (E_\psi - E_{\psi'})/\hbar$ . Relation (B1) follows by the Hermiticity of the current. This result is analytically continued to complex  $\omega$ .

In our model, the Hamiltonian is given approximately near the  $K$ - or  $K'$ -valley. Each of these Hamiltonians is not  $\mathcal{T}$ -symmetric. Since the total Hamiltonian is  $\mathcal{T}$ -symmetric, we apply the symmetrization

$$\sigma_{\nu\nu'}^{\ell\ell'}(\omega) = (\sigma_{\nu\nu',K}^{\ell\ell'}(\omega) + \sigma_{\nu'\nu,K}^{\ell'\ell}(\omega))/2, \quad (\text{B2})$$

where  $\sigma_{\nu\nu',K}^{\ell\ell'}$  is due to the  $K$  valley. The resulting conductivity formulas will include the valley degeneracy factor,  $g_v = 2$ ; and a spin degeneracy factor,  $g_s = 2$ .

### Appendix C: Optical conductivity of alternating-twist trilayer system: Calculations

In this appendix, we determine the optical conductivity for the alternating trilayer system by the Kubo formulation. The main assumptions are time reversal symmetry and spatial isotropy. We will invoke the unitary transformation of the  $K$ -valley trilayer Hamiltonian into a direct sum of the effective Hamiltonians  $\mathcal{H}_1$  and  $\mathcal{H}_2$  (Appendix A).<sup>45</sup> We will also use moiré-scaled quantities, so that the units of length and energy are  $\{2k_D \sin(\theta/2)\}^{-1}$  and  $2v_F \hbar k_D \sin(\theta/2)$ . Hence, the (dimensionless) current operator in layer  $\ell$  is  $\mathbf{j}^\ell = -i[\mathbf{x}^\ell, \mathcal{H}^{tri}]$ , where  $\mathcal{H}^{tri}$  and  $\mathbf{x}^\ell$  are the moiré-scaled trilayer Hamiltonian and vector position. For ease of notation, we often suppress the subscript  $K$ .

#### 1. Methodology and general results

We transform the unperturbed trilayer Hamiltonian,  $\mathcal{H}_K^{tri}$ , by  $\mathfrak{S}$  into the direct sum  $\mathcal{H}_2 \oplus \mathcal{H}_1$ . Hence, we compute the trace of the current-current commutators on the basis formed by the eigenvectors of  $\mathcal{H}_2 \oplus \mathcal{H}_1$ .

Consider the set of all state vectors of the form

$$|\underline{\psi}\rangle = \mathfrak{S}^\dagger |\psi\rangle = \begin{pmatrix} |b\rangle_1 \\ |b\rangle_2 \\ 0 \end{pmatrix} \quad \text{or} \quad \begin{pmatrix} 0 \\ 0 \\ |s\rangle \end{pmatrix},$$

which are eigenvectors of  $\mathcal{H}_2 \oplus \mathcal{H}_1$ ;  $|b\rangle = (|b\rangle_1, |b\rangle_2)^T$  and  $|s\rangle$  denote the effective twisted-bilayer and single-layer Hamiltonian eigenvectors, with energies  $E_b = E_b^{(2)}$  and  $E_s = E_s^{(1)}$ . The symbols  $b$  and  $s$  express the combined band index and quasi-momentum in the scaled moiré Brillouin zone.

For real  $\omega$ , the  $K$ -valley Kubo formula yields

$$\begin{aligned} \sigma_{\nu\nu',K}^{\ell\ell'}(\omega) &= C_0 \frac{e^2}{\hbar(\omega + i\delta)} \sum_{\{|\psi\rangle\}} f(E_\psi) \int_0^\infty dt e^{i(\omega+i\delta)t} \\ &\quad \times \langle \underline{\psi} | [\underline{j}_{\nu,K}^\ell(t), \underline{j}_{\nu',K}^{\ell'}(0)] | \underline{\psi} \rangle \\ &= C_0 \frac{e^2}{\hbar(\omega + i\delta)} \left\{ \sum_b f_b \int_0^\infty dt e^{i(\omega+i\delta)t} \right. \\ &\quad \times ({}_1\langle b|, {}_2\langle b|) (V_{bb,\nu\nu'}^{\ell\ell'}(t) - V_{bb,\nu\nu'}^{\ell\ell'}(t)^\dagger) \begin{pmatrix} |b\rangle_1 \\ |b\rangle_2 \end{pmatrix} \\ &\quad + \sum_s f_s \int_0^\infty dt e^{i(\omega+i\delta)t} \\ &\quad \times \langle s | V_{ss,\nu\nu'}^{\ell\ell'}(t) - V_{ss,\nu\nu'}^{\ell\ell'}(t)^\dagger | s \rangle \left. \right\}, \quad \delta \downarrow 0, \quad (\text{C1}) \end{aligned}$$

for  $\ell, \ell' = 1, 2, 3$  and  $\nu, \nu' = x, y$ . The  $\nu$ -directed current  $\underline{j}_{\nu,K}^\ell(t) = \mathfrak{S}^\dagger j_{\nu,K}^\ell(t) \mathfrak{S}$ , frequency  $\omega$  and time  $t$  are moiré scaled and dimensionless; and  $C_0 = \{4k_D^2 \sin^2(\theta/2) A_m\}^{-1} = \frac{3\sqrt{3}}{8\pi^2}$  where  $A_m = \frac{3\sqrt{3}}{8} \left(\frac{a_C}{\sin(\theta/2)}\right)^2$  is the area of the moiré cell and  $a_C$  is the carbon-carbon distance. We set  $f_\eta = f(E_\eta)$  as the Fermi-Dirac distribution, and  $V_{\eta\eta',\nu\nu'}^{\ell\ell'}(t) = \mathbf{e}_\nu \cdot \mathbf{V}_{\eta\eta'}^{\ell\ell'}(t) \cdot \mathbf{e}_{\nu'}$  ( $\mathbf{e}_\nu$ : Cartesian unit vector) for  $\eta, \eta' = b, s$ . The matrix-valued operator  $\mathbf{V}_{\eta\eta'}^{\ell\ell'}(t)$  is defined by

$$\underline{j}_K^\ell(t) \underline{j}_{0,K}^{\ell'} = \begin{pmatrix} \mathbf{V}_{bb}^{\ell\ell'}(t) & \mathbf{V}_{bs}^{\ell\ell'}(t) \\ \mathbf{V}_{sb}^{\ell\ell'}(t) & \mathbf{V}_{ss}^{\ell\ell'}(t) \end{pmatrix}, \quad (\text{C2})$$

and thus vanishes for  $t < 0$ ;  $\mathbf{j}_0^\ell = \mathbf{j}^\ell(0)$ . By Eq. (C1), we only need the diagonal terms,  $\mathbf{V}_{\eta\eta}^{\ell\ell'}(t)$ . The symbol  $\sum_\eta$  ( $\eta = b, s$ ) means summation over band indices and integration in the quasi-momentum over the scaled Brillouin zone. The elements  $\langle \eta | \cdot | \eta \rangle$  ( $\eta = b, s$ ) of Eq. (C1) account for  $\mathbf{x}$ -inner products of scalar Bloch wave functions, which compose  $\langle \mathbf{x} | \eta \rangle$ .

In Eq. (C1), each sum  $\sum_\eta$  is replaced by  $\sum_{\eta,\bar{\eta}'}$  or  $\sum_{\eta,\bar{\eta}}$  by use of the resolution of the identity,  $1 = \sum_\eta |\eta\rangle \langle \eta|$ , in the respective Hilbert space (for  $\eta = b, s$ ). Here, we set  $(\eta, \eta') = (b, b')$  or  $(s, s')$ , while  $\bar{\eta}'$  in  $(\eta, \bar{\eta}')$  takes values complementary to those of  $\eta$  in the sense that  $\bar{\eta}' = s'$  if  $\eta = b$  and  $\bar{\eta}' = b'$  if  $\eta = s$ .

For every  $\eta$  in these sums, the Fourier transform of  $\langle \eta | V_{\eta\eta,\nu\nu'}^{\ell\ell'}(t) | \eta \rangle$  contributes the factors

$$-\frac{1}{i(\omega + \omega_{\eta\eta'} + i\delta)} \quad \text{or} \quad -\frac{1}{i(\omega + \omega_{\eta\bar{\eta}'} + i\delta)},$$

as  $\delta \downarrow 0$ . The Fourier transform of  $\langle \eta | V_{\eta\eta,\nu\nu'}^{\ell\ell'}(t)^\dagger | \eta \rangle$  contributes the respective factors

$$-\frac{1}{i(\omega - \omega_{\eta\eta'} + i\delta)} \quad \text{or} \quad -\frac{1}{i(\omega - \omega_{\eta\bar{\eta}'} + i\delta)}.$$

The ensuing optical conductivity tensor,  $\boldsymbol{\sigma}(\omega)$ , comes from the symmetrization of the  $K$ -valley contribution (Appendix B). This  $\boldsymbol{\sigma}$  reads

$$\boldsymbol{\sigma}(\omega) = \begin{pmatrix} \boldsymbol{\sigma}^{11}(\omega) & \boldsymbol{\sigma}^{12}(\omega) & \boldsymbol{\sigma}^{13}(\omega) \\ \boldsymbol{\sigma}^{21}(\omega) & \boldsymbol{\sigma}^{22}(\omega) & \boldsymbol{\sigma}^{23}(\omega) \\ \boldsymbol{\sigma}^{31}(\omega) & \boldsymbol{\sigma}^{32}(\omega) & \boldsymbol{\sigma}^{33}(\omega) \end{pmatrix},$$

where  $\boldsymbol{\sigma}^{\ell\ell'}$  are  $2 \times 2$  matrices for the layer-resolved conductivities. We will express  $\boldsymbol{\sigma}^{\ell\ell'}$  in terms of principal conductivities associated with two effective, simpler systems, for *arbitrary* positive parameters  $\alpha_{12(23)}$  of the trilayer Hamiltonian  $\mathcal{H}_K^{tri}$  (Appendix A).

After some algebra, we obtain (see Sec. C3)

$$\boldsymbol{\sigma}^{11} = \lambda^{-4}(\alpha_{12}^4 \boldsymbol{\sigma}_{BL}^{11} + \alpha_{23}^4 \boldsymbol{\sigma}_{SL} + \alpha_{12}^2 \alpha_{23}^2 \boldsymbol{\sigma}_c) \quad (\text{C3})$$

$$= \begin{pmatrix} \sigma_0^{11} & 0 \\ 0 & \sigma_0^{11} \end{pmatrix}, \quad (\text{C4})$$

$$\begin{aligned} \boldsymbol{\sigma}^{12} &= \frac{\alpha_{12}^2}{\lambda^2} \boldsymbol{\sigma}_{BL}^{12} \\ &= \begin{pmatrix} \sigma_0^{12} & \sigma_{xy}^{12} \\ -\sigma_{xy}^{12} & \sigma_0^{12} \end{pmatrix} = (\boldsymbol{\sigma}^{21})^T, \end{aligned} \quad (\text{C5})$$

$$\boldsymbol{\sigma}^{13} = \frac{\alpha_{12}^2 \alpha_{23}^2}{\lambda^4} (\boldsymbol{\sigma}_{BL}^{11} + \boldsymbol{\sigma}_{SL} - \boldsymbol{\sigma}_c) \quad (\text{C6})$$

$$= \begin{pmatrix} \sigma_0^{13} & 0 \\ 0 & \sigma_0^{13} \end{pmatrix} = \boldsymbol{\sigma}^{31}, \quad (\text{C7})$$

$$\boldsymbol{\sigma}^{22} = \boldsymbol{\sigma}_{BL}^{22} = \begin{pmatrix} \sigma_0^{22} & 0 \\ 0 & \sigma_0^{22} \end{pmatrix}, \quad (\text{C8})$$

$$\begin{aligned} \boldsymbol{\sigma}^{23} &= \frac{\alpha_{23}^2}{\lambda^2} \boldsymbol{\sigma}_{BL}^{21} \\ &= \frac{\alpha_{23}^2}{\alpha_{12}^2} \boldsymbol{\sigma}^{21} = (\boldsymbol{\sigma}^{32})^T, \end{aligned} \quad (\text{C9})$$

$$\begin{aligned} \boldsymbol{\sigma}^{33} &= \lambda^{-4}(\alpha_{23}^4 \boldsymbol{\sigma}_{BL}^{11} + \alpha_{12}^4 \boldsymbol{\sigma}_{SL} + \alpha_{12}^2 \alpha_{23}^2 \boldsymbol{\sigma}_c) \\ &= \boldsymbol{\sigma}^{11}|_{\alpha_{12} \leftrightarrow \alpha_{23}} = \begin{pmatrix} \sigma_0^{33} & 0 \\ 0 & \sigma_0^{33} \end{pmatrix}. \end{aligned} \quad (\text{C10})$$

The first equation for  $\boldsymbol{\sigma}^{33}$  comes from interchanging the constants  $\alpha_{12}$  and  $\alpha_{23}$  in  $\boldsymbol{\sigma}^{11}$ . In Eqs. (C3)–(C10), we express the layer-resolved conductivities in terms of the principal  $2 \times 2$  matrices  $\boldsymbol{\sigma}_{BL}^{\zeta\zeta'}$ ,  $\boldsymbol{\sigma}_{SL}$ , and  $\boldsymbol{\sigma}_c$  ( $\zeta, \zeta' = 1, 2$ ). Here,  $\boldsymbol{\sigma}_{BL}^{\zeta\zeta'}$  and  $\boldsymbol{\sigma}_{SL}$  are conductivities that separately arise from the effective twisted bilayer and single-layer Hamiltonians, respectively; cf. Eqs. (A15) and (A14) in Appendix A. On the other hand,  $\boldsymbol{\sigma}_c$  couples the two effective systems.

The principal matrices have the forms

$$\boldsymbol{\sigma}_{SL} = \begin{pmatrix} \sigma_e^{(1)} & 0 \\ 0 & \sigma_e^{(1)} \end{pmatrix},$$

$$\boldsymbol{\sigma}_{BL}^{\zeta\zeta'} = \begin{pmatrix} \sigma_e^{(2)} & 0 \\ 0 & \sigma_e^{(2)} \end{pmatrix} \quad (\zeta = 1, 2),$$

$$\boldsymbol{\sigma}_{BL}^{12} = \begin{pmatrix} \sigma_e^{12} & \sigma_{e,xy}^{12} \\ -\sigma_{e,xy}^{12} & \sigma_e^{12} \end{pmatrix} = (\boldsymbol{\sigma}_{BL}^{21})^T,$$

$$\boldsymbol{\sigma}_c = \begin{pmatrix} \sigma_{0c} & 0 \\ 0 & \sigma_{0c} \end{pmatrix}.$$

The scalars  $\sigma_e^{(1,2)}$ ,  $\sigma_e^{12}$ ,  $\sigma_{e,xy}^{12}$ , and  $\sigma_{0c}$  respectively denote the in-plane conductivities of the effective single-layer and twisted bilayer systems, the covalent drag and chiral (or Hall) conductivities of the effective bilayer system, and the coupling of the two systems. Note that  $\sigma_0^{22} = \sigma_e^{(2)}$  in Eq. (C8). In Sec. C3, we express all these scalar functions of  $\omega$  in terms of inner products of suitable pseudo-spin wave functions.

Hence, the elements  $\sigma_0^{\ell\ell'}$  of Eqs. (C3)–(C10) are

$$\sigma_0^{11} = \lambda^{-4}(\alpha_{12}^4 \sigma_e^{(2)} + \alpha_{23}^4 \sigma_e^{(1)} + \alpha_{12}^2 \alpha_{23}^2 \sigma_{0c}), \quad (\text{C11})$$

$$\sigma_0^{12} = \frac{\alpha_{12}^2}{\lambda^2} \sigma_e^{12}, \quad \sigma_{xy}^{12} = \frac{\alpha_{12}^2}{\lambda^2} \sigma_{e,xy}^{12}, \quad (\text{C12})$$

$$\sigma_0^{13} = \frac{\alpha_{12}^2 \alpha_{23}^2}{\lambda^4} (\sigma_e^{(2)} + \sigma_e^{(1)} - \sigma_{0c}), \quad (\text{C13})$$

$$\sigma_0^{22} = \sigma_e^{(2)}, \quad (\text{C14})$$

$$\begin{aligned} \sigma_0^{33} &= \lambda^{-4}(\alpha_{23}^4 \sigma_e^{(2)} + \alpha_{12}^4 \sigma_e^{(1)} + \alpha_{23}^2 \alpha_{12}^2 \sigma_{0c}) \\ &= \sigma_0^{11}|_{\alpha_{12} \leftrightarrow \alpha_{23}}. \end{aligned} \quad (\text{C15})$$

In particular, let us consider  $\alpha_{12} = \alpha_{23}$ , by which mirror symmetry is recovered. We find

$$\boldsymbol{\sigma}^{11} = \frac{1}{4}(\boldsymbol{\sigma}_{BL}^{11} + \boldsymbol{\sigma}_{SL} + \boldsymbol{\sigma}_c), \quad (\text{C16})$$

$$\boldsymbol{\sigma}^{12} = \frac{1}{2} \boldsymbol{\sigma}_{BL}^{12} = (\boldsymbol{\sigma}^{21})^T, \quad (\text{C17})$$

$$\boldsymbol{\sigma}^{13} = \frac{1}{4}(\boldsymbol{\sigma}_{BL}^{11} + \boldsymbol{\sigma}_{SL} - \boldsymbol{\sigma}_c) = \boldsymbol{\sigma}^{31}, \quad (\text{C18})$$

$$\boldsymbol{\sigma}^{23} = \frac{1}{2} \boldsymbol{\sigma}_{BL}^{21} = \boldsymbol{\sigma}^{21} = (\boldsymbol{\sigma}^{32})^T, \quad (\text{C19})$$

$$\boldsymbol{\sigma}^{33} = \boldsymbol{\sigma}^{11}. \quad (\text{C20})$$

## 2. Trace algebra

Next, we provide details on the layer-resolved conductivities. We compute the unitarily transformed currents and  $\mathbf{V}_{\eta\eta'}^{\ell\ell'}(t)$  in view of Eq. (A11) of Appendix A and time evolution under Hamiltonian  $\mathcal{H}_K^{eff}$ .

The trace of the Kubo formula is computed on the basis formed by the eigenvectors of  $\mathcal{H}^{eff} = \mathcal{H}_2 \oplus \mathcal{H}_1$ . The unitarily transformed currents are

$$\underline{j}_{0\nu}^\ell = \mathfrak{S}^\dagger j_{0\nu}^\ell \mathfrak{S}, \quad \underline{j}_\nu^\ell(t) = e^{i\mathcal{H}^{eff}t} \underline{j}_{0\nu}^\ell e^{-i\mathcal{H}^{eff}t}.$$

The initial original (non-transformed)  $\nu$ -directed current in layer  $\ell$  is  $j_{0\nu}^\ell = \mathbf{j}_0^\ell \cdot \mathbf{e}_\nu$  with  $\mathbf{j}_0^\ell = -i[\mathbf{x}^\ell, \mathcal{H}^{tri}]$ , where  $\mathbf{e}_\nu$  is a Cartesian unit vector in the  $xy$ -plane.

Therefore, we start with the matrix representations

$$\mathbf{j}_0^1 = \begin{pmatrix} \tau^{-\theta} & 0 & 0 \\ 0 & 0 & 0 \\ 0 & 0 & 0 \end{pmatrix}, \quad \mathbf{j}_0^2 = \begin{pmatrix} 0 & 0 & 0 \\ 0 & \tau^\theta & 0 \\ 0 & 0 & 0 \end{pmatrix},$$

$$\mathbf{j}_0^3 = \begin{pmatrix} 0 & 0 & 0 \\ 0 & 0 & 0 \\ 0 & 0 & \tau^{-\theta} \end{pmatrix}.$$

We have defined

$$\tau^\theta = e^{(i/4)\theta\tau_z} \tau e^{-(i/4)\theta\tau_z}, \quad \tau = \tau_x \mathbf{e}_x + \tau_y \mathbf{e}_y,$$

where  $\tau_\nu$  is the  $\nu$ -Pauli matrix.

We need to compute

$$\underline{j}^\ell(t) = \begin{pmatrix} e^{i\mathcal{H}_2 t} & 0 \\ 0 & e^{i\mathcal{H}_1 t} \end{pmatrix} \underline{j}_0^\ell \begin{pmatrix} e^{-i\mathcal{H}_2 t} & 0 \\ 0 & e^{-i\mathcal{H}_1 t} \end{pmatrix}$$

in the matrix representation  $|L\rangle\langle L'|$ , where each of  $|L\rangle$  and  $|L'\rangle$  is  $(|b\rangle_1, |b\rangle_2, 0)^T$  or  $(0, 0, |s\rangle)^T$  ( $\ell = 1, 2, 3$ ). For the initial  $\mathfrak{S}$ -transformed currents, we find

$$\underline{j}_0^1 = \begin{pmatrix} \frac{\alpha_{12}^2}{\lambda^2} \tau_1 & \frac{\alpha_{12}\alpha_{23}}{\lambda^2} \tau_c \\ \frac{\alpha_{12}\alpha_{23}}{\lambda^2} \tau_c^\dagger & \left(\frac{\alpha_{23}}{\lambda}\right)^2 \tau^{-\theta} \end{pmatrix} \quad (\text{C21})$$

$$= \frac{1}{2} \begin{pmatrix} \tau_1 & \tau_c \\ \tau_c^\dagger & \tau^{-\theta} \end{pmatrix} \quad \text{if } \alpha_{12} = \alpha_{23},$$

$$\underline{j}_0^2 = \begin{pmatrix} \tau_2 & 0 \\ 0 & 0 \end{pmatrix}, \quad (\text{C22})$$

$$\underline{j}_0^3 = \begin{pmatrix} \frac{\alpha_{23}^2}{\lambda^2} \tau_1 & -\frac{\alpha_{12}\alpha_{23}}{\lambda^2} \tau_c \\ -\frac{\alpha_{12}\alpha_{23}}{\lambda^2} \tau_c^\dagger & \frac{\alpha_{12}^2}{\lambda^2} \tau^{-\theta} \end{pmatrix} \quad (\text{C23})$$

$$= \frac{1}{2} \begin{pmatrix} \tau_1 & -\tau_c \\ -\tau_c^\dagger & \tau^{-\theta} \end{pmatrix} \quad \text{if } \alpha_{12} = \alpha_{23},$$

where

$$\tau_1 = \begin{pmatrix} \tau^{-\theta} & 0 \\ 0 & 0 \end{pmatrix}, \quad \tau_2 = \begin{pmatrix} 0 & 0 \\ 0 & \tau^\theta \end{pmatrix},$$

$$\tau_c = \begin{pmatrix} \tau^{-\theta} \\ 0 \end{pmatrix}.$$

Thus, in the interaction picture we have

$$\underline{j}^1(t) = \frac{1}{\lambda^2} \begin{pmatrix} \alpha_{12}^2 e^{i\mathcal{H}_2 t} \tau_1 e^{-i\mathcal{H}_2 t} & \alpha_{12}\alpha_{23} e^{i\mathcal{H}_2 t} \tau_c e^{-i\mathcal{H}_1 t} \\ \alpha_{12}\alpha_{23} e^{i\mathcal{H}_1 t} \tau_c^\dagger e^{-i\mathcal{H}_2 t} & \alpha_{23}^2 e^{i\mathcal{H}_1 t} \tau^{-\theta} e^{-i\mathcal{H}_1 t} \end{pmatrix}, \quad \underline{j}^2(t) = \begin{pmatrix} e^{i\mathcal{H}_2 t} \tau_2 e^{-i\mathcal{H}_2 t} & 0 \\ 0 & 0 \end{pmatrix},$$

$$\underline{j}^3(t) = \frac{1}{\lambda^2} \begin{pmatrix} \alpha_{23}^2 e^{i\mathcal{H}_2 t} \tau_1 e^{-i\mathcal{H}_2 t} & -\alpha_{12}\alpha_{23} e^{i\mathcal{H}_2 t} \tau_c e^{-i\mathcal{H}_1 t} \\ -\alpha_{12}\alpha_{23} e^{i\mathcal{H}_1 t} \tau_c^\dagger e^{-i\mathcal{H}_2 t} & \alpha_{12}^2 e^{i\mathcal{H}_1 t} \tau^{-\theta} e^{-i\mathcal{H}_1 t} \end{pmatrix}.$$

By abusing notation, we define

$$\omega_{\eta\eta'} = E_\eta - E_{\eta'},$$

where  $E_\eta$  and  $E_{\eta'}$  denote eigen-energies of the effective single-layer or twisted bilayer systems. Notice that  $\omega_{bs}$  mixes these energies, and will appear in  $\sigma_c$  (Sec. C3).

Let us now outline the steps for the remaining computation of  $[\underline{j}^\ell(t), \underline{j}_0^{\ell'}]$ . For every pair  $(\ell, \ell')$  we use the matrices  $\mathbf{V}_{\eta\eta'}^{\ell\ell'}$  from Eq. (C2), needed for  $\eta = \eta'$ . Note that the Hermitian adjoint of this expression reads

$$\underline{j}_0^{\ell'} \underline{j}^\ell(t) = \begin{pmatrix} \mathbf{V}_{bb}^{\ell\ell'}(t)^\dagger & \mathbf{V}_{sb}^{\ell\ell'}(t)^\dagger \\ \mathbf{V}_{bs}^{\ell\ell'}(t)^\dagger & \mathbf{V}_{ss}^{\ell\ell'}(t)^\dagger \end{pmatrix}.$$

Thus, it suffices to determine  $\underline{j}^\ell(t) \underline{j}_0^{\ell'}$ . The matrix elements of  $[\underline{j}^\ell(t), \underline{j}_0^{\ell'}]$  are found from  $\mathbf{V}_{\eta\eta'}^{\ell\ell'}(t) - (\mathbf{V}_{\eta\eta'}^{\ell\ell'}(t))^\dagger$ .

#### a. Tensor $\mathbf{V}_{\eta\eta'}^{11}$

For  $(\ell, \ell') = (1, 1)$ , the diagonal block matrix of the first layer,  $[\underline{j}^1(t), \underline{j}_0^1]$  directly comes from the following formulas. Regarding  $\underline{j}^1(t) \underline{j}_0^1$ , we compute

$$\mathbf{V}_{bb}^{11} = \frac{\alpha_{12}^2}{\lambda^4} (\alpha_{12}^2 e^{i\mathcal{H}_2 t} \tau_1 e^{-i\mathcal{H}_2 t} \tau_1 + \alpha_{23}^2 e^{i\mathcal{H}_2 t} \tau_c \times e^{-i\mathcal{H}_1 t} \tau_c^\dagger),$$

$$\mathbf{V}_{bs}^{11} = \frac{\alpha_{12}\alpha_{23}}{\lambda^4} (\alpha_{12}^2 e^{i\mathcal{H}_2 t} \tau_1 e^{-i\mathcal{H}_2 t} \tau_c + \alpha_{23}^2 e^{i\mathcal{H}_2 t} \tau_c \times e^{-i\mathcal{H}_1 t} \tau^{-\theta}),$$

$$\mathbf{V}_{sb}^{11} = \frac{\alpha_{12}\alpha_{23}}{\lambda^4} \left( \alpha_{12}^2 e^{i\mathcal{H}_1 t} \boldsymbol{\tau}_c^\dagger e^{-i\mathcal{H}_2 t} \boldsymbol{\tau}_1 + \alpha_{23}^2 e^{i\mathcal{H}_1 t} \boldsymbol{\tau}^{-\theta} \right. \\ \left. \times e^{-i\mathcal{H}_1 t} \boldsymbol{\tau}_c^\dagger \right),$$

$$\mathbf{V}_{ss}^{11} = \frac{\alpha_{23}^2}{\lambda^4} \left( \alpha_{12}^2 e^{i\mathcal{H}_1 t} \boldsymbol{\tau}_c^\dagger e^{-i\mathcal{H}_2 t} \boldsymbol{\tau}_c + \alpha_{23}^2 e^{i\mathcal{H}_1 t} \boldsymbol{\tau}^{-\theta} \right. \\ \left. \times e^{-i\mathcal{H}_1 t} \boldsymbol{\tau}^{-\theta} \right).$$

The product  $\underline{\mathbf{j}}_0^1 \mathbf{j}^1(t)$  is thus determined by

$$(\mathbf{V}_{bb}^{11})^\dagger = \frac{\alpha_{12}^2}{\lambda^4} \left( \alpha_{12}^2 \boldsymbol{\tau}_1 e^{i\mathcal{H}_2 t} \boldsymbol{\tau}_1 e^{-i\mathcal{H}_2 t} + \alpha_{23}^2 \boldsymbol{\tau}_c \right. \\ \left. \times e^{i\mathcal{H}_1 t} \boldsymbol{\tau}_c^\dagger e^{-i\mathcal{H}_2 t} \right),$$

$$(\mathbf{V}_{sb}^{11})^\dagger = \frac{\alpha_{12}\alpha_{23}}{\lambda^4} \left( \alpha_{12}^2 \boldsymbol{\tau}_1 e^{i\mathcal{H}_2 t} \boldsymbol{\tau}_c e^{-i\mathcal{H}_1 t} + \alpha_{23}^2 \boldsymbol{\tau}_c \right. \\ \left. \times e^{i\mathcal{H}_1 t} \boldsymbol{\tau}^{-\theta} e^{-i\mathcal{H}_1 t} \right),$$

$$(\mathbf{V}_{bs}^{11})^\dagger = \frac{\alpha_{12}\alpha_{23}}{\lambda^4} \left( \alpha_{12}^2 \boldsymbol{\tau}_c^\dagger e^{i\mathcal{H}_2 t} \boldsymbol{\tau}_1 e^{-i\mathcal{H}_2 t} + \alpha_{23}^2 \boldsymbol{\tau}^{-\theta} \right. \\ \left. \times e^{i\mathcal{H}_1 t} \boldsymbol{\tau}_c^\dagger e^{-i\mathcal{H}_2 t} \right),$$

$$(\mathbf{V}_{ss}^{11})^\dagger = \frac{\alpha_{23}^2}{\lambda^4} \left( \alpha_{12}^2 \boldsymbol{\tau}_c^\dagger e^{i\mathcal{H}_2 t} \boldsymbol{\tau}_c e^{-i\mathcal{H}_1 t} + \alpha_{23}^2 \boldsymbol{\tau}^{-\theta} \right. \\ \left. \times e^{i\mathcal{H}_1 t} \boldsymbol{\tau}^{-\theta} e^{-i\mathcal{H}_1 t} \right).$$

The commutator  $[\underline{\mathbf{j}}^1(t), \underline{\mathbf{j}}_0^1]$  is then readily computed.

b. *Tensors  $\mathbf{V}_{\eta\eta'}^{12}$  and  $\mathbf{V}_{\eta\eta'}^{21}$*

Let us now discuss the structure of both  $[\underline{\mathbf{j}}^1(t), \underline{\mathbf{j}}_0^2]$  and  $[\underline{\mathbf{j}}^2(t), \underline{\mathbf{j}}_0^1]$ . For the product  $\underline{\mathbf{j}}^1(t) \underline{\mathbf{j}}_0^2$ , we compute

$$\mathbf{V}_{bb}^{12} = \frac{\alpha_{12}^2}{\lambda^2} e^{i\mathcal{H}_2 t} \boldsymbol{\tau}_1 e^{-i\mathcal{H}_2 t} \boldsymbol{\tau}_2, \\ \mathbf{V}_{sb}^{12} = \frac{\alpha_{12}\alpha_{23}}{\lambda^2} e^{i\mathcal{H}_1 t} \boldsymbol{\tau}_c^\dagger e^{-i\mathcal{H}_2 t} \boldsymbol{\tau}_2, \\ \mathbf{V}_{bs}^{12} = 0 = \mathbf{V}_{ss}^{12}.$$

Similarly, for  $\underline{\mathbf{j}}_0^2 \mathbf{j}^1(t)$  we invoke the Hermitian conjugate (adjoint) of each of the above quantities.

For  $[\underline{\mathbf{j}}^2(t), \underline{\mathbf{j}}_0^1]$ , a similar calculation yields

$$\mathbf{V}_{bb}^{21} = \frac{\alpha_{12}^2}{\lambda^2} e^{i\mathcal{H}_2 t} \boldsymbol{\tau}_2 e^{-i\mathcal{H}_2 t} \boldsymbol{\tau}_1, \\ \mathbf{V}_{bs}^{21} = \frac{\alpha_{12}\alpha_{23}}{\lambda^2} e^{i\mathcal{H}_2 t} \boldsymbol{\tau}_2 e^{-i\mathcal{H}_2 t} \boldsymbol{\tau}_c, \\ \mathbf{V}_{sb}^{21} = 0 = \mathbf{V}_{ss}^{21}.$$

The Hermitian conjugate of each term follows directly.

c. *Tensors  $\mathbf{V}_{\eta\eta'}^{13}$  and  $\mathbf{V}_{\eta\eta'}^{31}$*

Next, we focus on  $[\underline{\mathbf{j}}^1(t), \underline{\mathbf{j}}_0^3]$  and  $[\underline{\mathbf{j}}^3(t), \underline{\mathbf{j}}_0^1]$ . For the former, the product  $\underline{\mathbf{j}}^1(t) \underline{\mathbf{j}}_0^3$  is composed of

$$\mathbf{V}_{bb}^{13} = \frac{\alpha_{12}^2 \alpha_{23}^2}{\lambda^4} \left( e^{i\mathcal{H}_2 t} \boldsymbol{\tau}_1 e^{-i\mathcal{H}_2 t} \boldsymbol{\tau}_1 - e^{i\mathcal{H}_2 t} \boldsymbol{\tau}_c e^{-i\mathcal{H}_1 t} \boldsymbol{\tau}_c^\dagger \right), \\ \mathbf{V}_{bs}^{13} = \frac{\alpha_{12}^3 \alpha_{23}}{\lambda^4} \left( e^{i\mathcal{H}_2 t} \boldsymbol{\tau}_c e^{-i\mathcal{H}_1 t} \boldsymbol{\tau}^{-\theta} - e^{i\mathcal{H}_2 t} \boldsymbol{\tau}_1 e^{-i\mathcal{H}_2 t} \boldsymbol{\tau}_c \right), \\ \mathbf{V}_{sb}^{13} = \frac{\alpha_{12} \alpha_{23}^3}{\lambda^4} \left( e^{i\mathcal{H}_1 t} \boldsymbol{\tau}_c^\dagger e^{-i\mathcal{H}_2 t} \boldsymbol{\tau}_1 - e^{i\mathcal{H}_1 t} \boldsymbol{\tau}^{-\theta} e^{-i\mathcal{H}_1 t} \boldsymbol{\tau}_c^\dagger \right), \\ \mathbf{V}_{ss}^{13} = \frac{\alpha_{12}^2 \alpha_{23}^2}{\lambda^4} \left( e^{i\mathcal{H}_1 t} \boldsymbol{\tau}^{-\theta} e^{-i\mathcal{H}_1 t} \boldsymbol{\tau}^{-\theta} - e^{i\mathcal{H}_1 t} \boldsymbol{\tau}_c^\dagger e^{-i\mathcal{H}_2 t} \boldsymbol{\tau}_c \right).$$

For  $\underline{\mathbf{j}}_0^3 \mathbf{j}^1(t)$ , we compute the Hermitian adjoints.

On the other hand, in regard to  $[\underline{\mathbf{j}}^3(t), \underline{\mathbf{j}}_0^1]$  we obtain

$$\mathbf{V}_{bb}^{31} = \frac{\alpha_{12}^2 \alpha_{23}^2}{\lambda^4} \left( e^{i\mathcal{H}_2 t} \boldsymbol{\tau}_1 e^{-i\mathcal{H}_2 t} \boldsymbol{\tau}_1 - e^{i\mathcal{H}_2 t} \boldsymbol{\tau}_c e^{-i\mathcal{H}_1 t} \boldsymbol{\tau}_c^\dagger \right), \\ \mathbf{V}_{bs}^{31} = \frac{\alpha_{12} \alpha_{23}^3}{\lambda^4} \left( e^{i\mathcal{H}_2 t} \boldsymbol{\tau}_1 e^{-i\mathcal{H}_2 t} \boldsymbol{\tau}_c - e^{i\mathcal{H}_2 t} \boldsymbol{\tau}_c e^{-i\mathcal{H}_1 t} \boldsymbol{\tau}^{-\theta} \right), \\ \mathbf{V}_{sb}^{31} = \frac{\alpha_{12}^3 \alpha_{23}}{\lambda^4} \left( e^{i\mathcal{H}_1 t} \boldsymbol{\tau}^{-\theta} e^{-i\mathcal{H}_1 t} \boldsymbol{\tau}_c^\dagger - e^{i\mathcal{H}_1 t} \boldsymbol{\tau}_c^\dagger e^{-i\mathcal{H}_2 t} \boldsymbol{\tau}_1 \right), \\ \mathbf{V}_{ss}^{31} = \frac{\alpha_{12}^2 \alpha_{23}^2}{\lambda^4} \left( e^{i\mathcal{H}_1 t} \boldsymbol{\tau}^{-\theta} e^{-i\mathcal{H}_1 t} \boldsymbol{\tau}^{-\theta} - e^{i\mathcal{H}_1 t} \boldsymbol{\tau}_c^\dagger e^{-i\mathcal{H}_2 t} \boldsymbol{\tau}_c \right),$$

along with their Hermitian conjugates. This step concludes the calculation for  $(\ell, \ell') = (1, 3), (3, 1)$ .

d. *Tensor  $\mathbf{V}_{\eta\eta'}^{22}$*

Consider the diagonal block matrix of the middle layer, related to  $[\underline{\mathbf{j}}^2(t), \underline{\mathbf{j}}_0^2]$ . For  $\underline{\mathbf{j}}^2(t) \underline{\mathbf{j}}_0^2$ , we need

$$\mathbf{V}_{bb}^{22} = e^{i\mathcal{H}_2 t} \boldsymbol{\tau}_2 e^{-i\mathcal{H}_2 t} \boldsymbol{\tau}_2, \\ \mathbf{V}_{bs}^{22} = 0 = \mathbf{V}_{sb}^{22} = \mathbf{V}_{ss}^{22}.$$

The Hermitian adjoint, for  $\underline{\mathbf{j}}_0^2 \mathbf{j}^2(t)$ , follows directly.

e. *Tensors  $\mathbf{V}_{\eta\eta'}^{23}$  and  $\mathbf{V}_{\eta\eta'}^{32}$*

For layers 2 and 3, we first compute

$$\mathbf{V}_{bb}^{23} = \frac{\alpha_{23}^2}{\lambda^2} e^{i\mathcal{H}_2 t} \boldsymbol{\tau}_2 e^{-i\mathcal{H}_2 t} \boldsymbol{\tau}_1, \\ \mathbf{V}_{bs}^{23} = -\frac{\alpha_{12}\alpha_{23}}{\lambda^2} e^{i\mathcal{H}_2 t} \boldsymbol{\tau}_2 e^{-i\mathcal{H}_2 t} \boldsymbol{\tau}_c, \\ \mathbf{V}_{sb}^{23} = 0 = \mathbf{V}_{ss}^{23}.$$

Likewise, we have

$$\mathbf{V}_{bb}^{32} = \frac{\alpha_{23}^2}{\lambda^2} e^{i\mathcal{H}_2 t} \boldsymbol{\tau}_1 e^{-i\mathcal{H}_2 t} \boldsymbol{\tau}_2, \\ \mathbf{V}_{sb}^{32} = -\frac{\alpha_{12}\alpha_{23}}{\lambda^2} e^{i\mathcal{H}_1 t} \boldsymbol{\tau}_c^\dagger e^{-i\mathcal{H}_2 t} \boldsymbol{\tau}_2, \\ \mathbf{V}_{bs}^{32} = 0 = \mathbf{V}_{ss}^{32}.$$

f. Tensor  $\mathbf{V}_{\eta\eta'}^{33}$

For the diagonal block matrix of the third (top) layer, a direct computation yields

$$\begin{aligned}\mathbf{V}_{bb}^{33} &= \frac{\alpha_{23}^2}{\lambda^4} (\alpha_{23}^2 e^{i\mathcal{H}_2 t} \boldsymbol{\tau}_1 e^{-i\mathcal{H}_2 t} \boldsymbol{\tau}_1 + \alpha_{12}^2 e^{i\mathcal{H}_2 t} \\ &\quad \times \boldsymbol{\tau}_c e^{-i\mathcal{H}_1 t} \boldsymbol{\tau}_c^\dagger) , \\ \mathbf{V}_{bs}^{33} &= -\frac{\alpha_{23}\alpha_{23}}{\lambda^4} (\alpha_{23}^2 e^{i\mathcal{H}_2 t} \boldsymbol{\tau}_1 e^{-i\mathcal{H}_2 t} \boldsymbol{\tau}_c + \alpha_{12}^2 e^{i\mathcal{H}_2 t} \\ &\quad \times \boldsymbol{\tau}_c e^{-i\mathcal{H}_1 t} \boldsymbol{\tau}^{-\theta}) , \\ \mathbf{V}_{sb}^{33} &= -\frac{\alpha_{23}\alpha_{23}}{\lambda^4} (\alpha_{23}^2 e^{i\mathcal{H}_1 t} \boldsymbol{\tau}_c^\dagger e^{-i\mathcal{H}_1 t} \boldsymbol{\tau}_1 + \alpha_{12}^2 e^{i\mathcal{H}_1 t} \\ &\quad \times \boldsymbol{\tau}^{-\theta} e^{-i\mathcal{H}_1 t} \boldsymbol{\tau}_c^\dagger) , \\ \mathbf{V}_{ss}^{33} &= \frac{\alpha_{12}^2}{\lambda^4} (\alpha_{23}^2 e^{i\mathcal{H}_1 t} \boldsymbol{\tau}_c^\dagger e^{-i\mathcal{H}_2 t} \boldsymbol{\tau}_c + \alpha_{12}^2 e^{i\mathcal{H}_1 t} \\ &\quad \times \boldsymbol{\tau}^{-\theta} e^{-i\mathcal{H}_1 t} \boldsymbol{\tau}^{-\theta}) .\end{aligned}$$

### 3. Layer-resolved conductivity matrices

Next, we outline the remaining steps of deriving the conductivity formulas of Sec. C 1 in this appendix. Let

$$\begin{aligned}|s\rangle &= (|\zeta_{s1}\rangle, |\zeta_{s2}\rangle)^T, \\ |b\rangle_1 &= (|\varphi_{b1}\rangle, |\varphi_{b2}\rangle)^T, \quad |b\rangle_2 = (|\chi_{b1}\rangle, |\chi_{b2}\rangle)^T,\end{aligned}$$

where  $\zeta_{si}(\mathbf{x}) = \langle \mathbf{x} | \zeta_{si} \rangle$ ,  $\varphi_{bi}(\mathbf{x}) = \langle \mathbf{x} | \varphi_{bi} \rangle$  and  $\chi_{bi}(\mathbf{x}) = \langle \mathbf{x} | \chi_{bi} \rangle$  ( $i = 1, 2$ ) are scalar Bloch wave functions. These are labeled by  $s$  or  $b$  for the combined band index and quasi-momentum variable of the scaled Brillouin zone. The spin degeneracy factor,  $g_s$ , will be omitted here but can be included in the end (Sec. III B).

#### a. $\sigma^{11}$ tensor

By Eq. (C1), the structure of  $\sigma^{11}$  is dictated by the tensors  $\mathbf{V}_{\eta\eta'}^{11}$ . For example, for  $\eta = b$  we have the term

$$\frac{\alpha_{12}^2}{\lambda^4} (\alpha_{12}^2 e^{i\mathcal{H}_2 t} \boldsymbol{\tau}_1 e^{-i\mathcal{H}_2 t} \boldsymbol{\tau}_1 + \alpha_{23}^2 e^{i\mathcal{H}_2 t} \boldsymbol{\tau}_c e^{-i\mathcal{H}_1 t} \boldsymbol{\tau}_c^\dagger) .$$

For  $\eta = s$ , the quantities  $\alpha_{12}$  and  $\alpha_{23}$ ,  $\mathcal{H}_1$  and  $\mathcal{H}_2$ ,  $\boldsymbol{\tau}_1$  and  $\boldsymbol{\tau}^{-\theta}$ , and  $\boldsymbol{\tau}_c$  and  $\boldsymbol{\tau}_c^\dagger$  must be respectively interchanged. By resolution of the identity, formula (C3) emerges once we identify the  $K$ -valley contributions

$$\begin{aligned}(\sigma_{BL,\nu\nu'}^{11})_K &= -C_0 \frac{e^2}{i\hbar\omega + i\delta} \sum_{bb'} (f_b - f_{b'}) \\ &\quad \times \frac{\langle b | \tau_{1\nu} | b' \rangle \langle b' | \tau_{1\nu'} | b \rangle}{\omega + \omega_{bb'} + i\delta},\end{aligned}\quad (\text{C24})$$

$$\begin{aligned}(\sigma_{SL,\nu\nu'})_K &= -C_0 \frac{e^2}{i\hbar\omega + i\delta} \sum_{ss'} (f_s - f_{s'}) \\ &\quad \times \frac{\langle s | \tau_{\nu}^{-\theta} | s' \rangle \langle s' | \tau_{\nu'}^{-\theta} | s \rangle}{\omega + \omega_{ss'} + i\delta},\end{aligned}\quad (\text{C25})$$

as  $\delta \downarrow 0$  for real  $\omega$ . Here, we set  $\tau_{(1)\nu}^{-\theta} = \mathbf{e}_\nu \cdot \boldsymbol{\tau}_{(1)}^{-\theta}$ . These formulas lead to the forms  $\boldsymbol{\sigma}_{SL} = \text{diag}(\sigma_e^{(1)}, \sigma_e^{(1)})$  and  $\boldsymbol{\sigma}_{BL}^{11} = \text{diag}(\sigma_e^{(2)}, \sigma_e^{(2)})$ , with the suitable definitions of the scalars  $\sigma_e^{(1,2)}$ . The coupling term  $\boldsymbol{\sigma}_c$  comes from the  $\boldsymbol{\tau}_c^{(\dagger)}$ -matrix terms in  $\mathbf{V}_{\eta\eta'}^{11}$ , viz. (with  $\tau_{c\nu} = \mathbf{e}_\nu \cdot \boldsymbol{\tau}_c$ ),

$$\begin{aligned}(\sigma_{c,\nu\nu'})_K &= -C_0 \frac{e^2}{i\hbar\omega + i\delta} \sum_{bs} (f_b - f_s) \\ &\quad \times \left\{ \frac{\langle b | \tau_{c\nu} | s \rangle \langle s | \tau_{c\nu'}^\dagger | b \rangle}{\omega + \omega_{bs} + i\delta} - \frac{\langle b | \tau_{c\nu'} | s \rangle \langle s | \tau_{c\nu}^\dagger | b \rangle}{\omega - \omega_{bs} + i\delta} \right\} .\end{aligned}$$

We proceed to symmetrize the above quantities. For the effective single-layer system, by isotropy we have the diagonal element  $\sigma_{SL,xx} = \sigma_{SL,yy} = \sigma_e^{(1)}$  with

$$\begin{aligned}\sigma_e^{(1)}(\omega) &= -i2C_0 g_v \frac{e^2}{\hbar(\omega + i\delta)} \sum_{ss'} (f_s - f_{s'}) \\ &\quad \times \frac{\omega_{ss'}}{(\omega + i\delta)^2 - \omega_{ss'}^2} |\langle \zeta_{s1} | \zeta_{s'2} \rangle|^2 .\end{aligned}$$

Here,  $g_v$  is the valley degeneracy factor ( $g_v = 2$ ) and  $\langle \zeta_{s1} | \zeta_{s'2} \rangle$  stands for the inner product of the scalar Bloch wave functions  $\zeta_{1,2}^{s,s'}(\mathbf{x})$  over the scaled cell. For the off-diagonal elements  $\sigma_{SL,xy}$  and  $\sigma_{SL,yx}$ , symmetrization and the effect of isotropy yield

$$\sigma_{SL,xy}(\omega) = -\sigma_{SL,yx}(\omega) = 0 .$$

Similarly, for the effective twisted bilayer system, by isotropy we have  $\sigma_{BL,xx}^{11} = \sigma_{BL,yy}^{11} = \sigma_e^{(2)}$  where

$$\begin{aligned}\sigma_e^{(2)}(\omega) &= -i2C_0 g_v \frac{e^2}{\hbar(\omega + i\delta)} \sum_{bb'} (f_b - f_{b'}) \\ &\quad \times \frac{\omega_{bb'}}{(\omega + i\delta)^2 - \omega_{bb'}^2} |\langle \varphi_{b1} | \varphi_{b'2} \rangle|^2 .\end{aligned}$$

The calculation for  $\sigma_{BL,xy}^{11}$  and  $\sigma_{BL,yx}^{11}$  makes explicit use of time reversal symmetry and isotropy, yielding

$$\sigma_{BL,xy}^{11}(\omega) = -\sigma_{BL,yx}^{11}(\omega) = 0 .$$

Let us consider  $\boldsymbol{\sigma}_c$ . For its diagonal elements, we get

$$\begin{aligned}(\sigma_{c,yy}^{xx})_K &= -2iC_0 \frac{e^2}{\hbar(\omega + i\delta)} \sum_{bs} (f_b - f_s) \\ &\quad \times \frac{\omega_{bs}}{(\omega + i\delta)^2 - \omega_{bs}^2} |\langle \check{\varphi}_{b1} | \zeta_{s2} \rangle \pm \langle \varphi_{b2} | \check{\zeta}_{s1} \rangle|^2 ,\end{aligned}$$



where  $\tilde{\omega} = e^{i\theta/2}\omega$  for  $\omega = \varphi_{b1}, \zeta_{s1}$ . By isotropy, we have  $\sigma_{c,xx}(\omega) - \sigma_{c,yy}(\omega) = 0$  which implies

$$\sum_{bs} (f_b - f_s) \frac{\omega_{bs}}{(\omega + i\delta)^2 - \omega_{bs}^2} \times \text{Re}(\langle \tilde{\varphi}_{b1} | \zeta_{s2} \rangle \langle \tilde{\zeta}_{s1} | \varphi_{b2} \rangle) = 0; \quad (\text{C26})$$

thus,  $\sigma_{c,xx} = \sigma_{c,yy} = \sigma_{0c}$  where

$$\sigma_{0c}(\omega) = -i2C_0g_v \frac{e^2}{\hbar(\omega + i\delta)} \sum_{bs} (f_b - f_s) \frac{\omega_{bs}}{(\omega + i\delta)^2 - \omega_{bs}^2} \times (|\langle \varphi_{b1} | \zeta_{s2} \rangle|^2 + |\langle \varphi_{b2} | \zeta_{s1} \rangle|^2). \quad (\text{C27})$$

This expression can be simplified by use of  $|\langle \varphi_{b1} | \zeta_{s2} \rangle| = |\langle \zeta_{s1} | \varphi_{b2} \rangle|$  due to the invariance of  $\mathcal{H}_{1,2}$  under the combined operations of sublattice index switch, complex conjugation, and parity inversion.

For the off-diagonal elements of  $\sigma_c$ , we assert that

$$(\sigma_{c,xy})_K = 2C_0 \frac{e^2}{\hbar(\omega + i\delta)} \sum_{bs} (f_b - f_s) \times \frac{\mp(\omega + i\delta)\text{Re}(m_{bs}^{\varphi\zeta}) + i\omega_{bs}\text{Im}(m_{bs}^{\varphi\zeta})}{(\omega + i\delta)^2 - \omega_{bs}^2}, \quad \delta \downarrow 0;$$

$$m_{bs}^{\varphi\zeta} = (\langle \tilde{\varphi}_{b1} | \zeta_{s2} \rangle + \langle \varphi_{b2} | \tilde{\zeta}_{s1} \rangle) (\langle \zeta_{s2} | \tilde{\varphi}_{b1} \rangle - \langle \tilde{\zeta}_{s1} | \varphi_{b2} \rangle).$$

By symmetrizing this  $K$ -valley contribution, we obtain

$$\sigma_{c,xy}(\omega) = \sigma_{c,yx}(\omega) = i2C_0g_v \frac{e^2}{\hbar(\omega + i\delta)} \times \sum_{bs} (f_b - f_s) \frac{\omega_{bs}}{(\omega + i\delta)^2 - \omega_{bs}^2} \text{Im}(m_{bs}^{\varphi\zeta}).$$

Notice that  $\text{Im}(m_{bs}^{\varphi\zeta}) = -2\text{Im}(\langle \tilde{\varphi}_{b1} | \zeta_{s2} \rangle \langle \tilde{\zeta}_{s1} | \varphi_{b2} \rangle)$ . By identity (C26), along with the interchange of the  $\text{Re}(\cdot)$  and  $\text{Im}(\cdot)$  in it, we infer that  $\sigma_{c,xy}(\omega) = 0 = \sigma_{c,yx}(\omega)$ . Alternatively, this vanishing of the off-diagonal elements of  $\sigma_c$  results from isotropy, by which  $\sigma_{c,xy}(\omega) = -\sigma_{c,yx}(\omega)$ . Equations (C4) and (C11) follow.

### b. $\sigma^{12}$ and $\sigma^{21}$ tensors

Next, we address the cases of layer pairs  $(\ell, \ell') = (1, 2), (2, 1)$ . Because each of  $\mathbf{V}_{bb'}^{12,21}$  contains only one product with  $\tau_{1,2}$  and is multiplied by  $\alpha_{12}^2\lambda^{-2}$ , while  $\mathbf{V}_{ss}^{12,21} = 0$ , we see that each of  $\sigma^{12,21}$  is proportional to  $\sigma_{BL}^{12,21}$ . For the  $K$ -valley term, Eq. (C1) implies

$$\sigma_K^{12(21)} = \frac{\alpha_{12}^2}{\lambda^2} (\sigma_{BL}^{12(21)})_K,$$

where

$$(\sigma_{BL,\nu\nu'}^{12(21)})_K = -C_0 \frac{e^2}{\hbar(\omega + i\delta)} \sum_{bb'} (f_b - f_{b'}) \times \frac{\langle b | \tau_{1(2)\nu} | b' \rangle \langle b' | \tau_{2(1)\nu'} | b \rangle}{i(\omega + i\delta + \omega_{bb'})}.$$

For the diagonal elements, symmetrization entails

$$\sigma_{BL,yy}^{12} = \sigma_{BL,yy}^{21} = -i2C_0g_v \frac{e^2}{\hbar(\omega + i\delta)} \sum_{bb'} (f_b - f_{b'}) \times \frac{\omega_{bb'} \text{Re} \{ (\langle \tilde{\varphi}_{b1} | \varphi_{b'2} \rangle \pm \langle \varphi_{b2} | \tilde{\varphi}_{b'1} \rangle) \langle \tilde{\chi}_{b'2} | \chi_{b1} \rangle \}}{(\omega + i\delta)^2 - \omega_{bb'}^2}.$$

By isotropy, which means  $\sigma_{BL,xx}^{12(21)} - \sigma_{BL,yy}^{12(21)} = 0$ , we have

$$\sum_{bb'} (f_b - f_{b'}) \frac{\omega_{bb'} \text{Re}(\langle \tilde{\varphi}_{b1} | \varphi_{b'2} \rangle \langle \chi_{b'2} | \tilde{\chi}_{b2} \rangle)}{(\omega + i\delta)^2 - \omega_{bb'}^2} = 0; \quad (\text{C28})$$

therefore, we can set  $\sigma_{BL,xx}^{12(21)} = \sigma_{BL,yy}^{12(21)} = \sigma_e^{12}$  where

$$\sigma_e^{12}(\omega) = -i2C_0g_v \frac{e^2}{\hbar(\omega + i\delta)} \sum_{bb'} (f_b - f_{b'}) \times \frac{\omega_{bb'} \text{Re}(e^{-i\theta} \langle \varphi_{b1} | \varphi_{b'2} \rangle \langle \chi_{b'2} | \chi_{b1} \rangle)}{(\omega + i\delta)^2 - \omega_{bb'}^2}. \quad (\text{C29})$$

Regarding the off-diagonal elements of  $\sigma^{12}$ , we find

$$\sigma_{BL,xy}^{12} = \sigma_{BL,xy}^{21} = \pm i2C_0g_v \frac{e^2}{\hbar(\omega + i\delta)} \sum_{bb'} (f_b - f_{b'}) \times \frac{\omega_{bb'} \text{Im} \{ (\langle \tilde{\chi}_{b'2} | \chi_{b1} \rangle \mp \langle \chi_{b'1} | \tilde{\chi}_{b2} \rangle) \langle \tilde{\varphi}_{b1} | \varphi_{b'2} \rangle \}}{(\omega + i\delta)^2 - \omega_{bb'}^2}$$

which express chirality. Note that  $\sigma_{BL,xy}^{12(21)} + \sigma_{BL,xy}^{12(21)} = 0$ , inferred from Eq. (C28) via replacement of  $\text{Re}(\cdot)$  by  $\text{Im}(\cdot)$ ; thus,  $\sigma_{BL,xy}^{12(21)} = -\sigma_{BL,xy}^{12(21)} = \sigma_{e,xy}^{12}$  with

$$\sigma_{e,xy}^{12}(\omega) = i2C_0g_v \frac{e^2}{\hbar(\omega + i\delta)} \sum_{bb'} (f_b - f_{b'}) \times \frac{\omega_{bb'} \text{Im}(e^{-i\theta} \langle \chi_{b'2} | \chi_{b1} \rangle \langle \varphi_{b1} | \varphi_{b'2} \rangle)}{(\omega + i\delta)^2 - \omega_{bb'}^2}. \quad (\text{C30})$$

### c. $\sigma^{13}$ and $\sigma^{31}$ tensors

Consider  $(\ell, \ell') = (1, 3)$  and  $(3, 1)$ . By Eq. (C1),  $\sigma^{13,31}$  contain contributions from the two effective systems and the coupling term  $\sigma_c$  that are similar to those for  $\sigma^{11}(\omega)$ . By inspection of  $\mathbf{V}_{\eta\eta}^{13,31}$  in comparison to  $\mathbf{V}_{\eta\eta}^{11}$ , from Eq. (C1) we can derive Eq. (C6).

In more detail, for  $\alpha_{12} = \alpha_{23}$ , we see that

$$\mathbf{V}_{bb}^{11} = \frac{1}{4} (e^{i\mathcal{H}_2 t} \tau_1 e^{-i\mathcal{H}_2 t} \tau_1 + e^{i\mathcal{H}_2 t} \tau_c e^{-i\mathcal{H}_1 t} \tau_c^\dagger)$$

whereas

$$\mathbf{V}_{bb}^{13} = \frac{1}{4} (e^{i\mathcal{H}_2 t} \tau_1 e^{-i\mathcal{H}_2 t} \tau_1 - e^{i\mathcal{H}_2 t} \tau_c e^{-i\mathcal{H}_1 t} \tau_c^\dagger) = \mathbf{V}_{bb}^{31};$$

ditto for  $\mathbf{V}_{ss}^{11,13}$  via the switch of  $\mathcal{H}_2$  and  $\mathcal{H}_1$ ,  $\tau_1$  and  $\tau^{-\theta}$ , and  $\tau_c$  and its Hermitian adjoint. Thus,

in the case with mirror symmetry, the matrix  $\sigma^{11}$  of Eq. (C16) is replaced by the  $\sigma^{13}$  given in Eq. (C18).

Now consider  $\alpha_{12} \neq \alpha_{23}$ . Notice the terms in

$$\mathbf{V}_{bb(ss)}^{11} = \frac{\alpha_{12}^2 \alpha_{23}^2}{\lambda^4} \left( \alpha_{12(23)}^2 e^{i\mathcal{H}_{2(1)}t} \boldsymbol{\tau}_1^{(-\theta)} e^{-i\mathcal{H}_{2(1)}t} \boldsymbol{\tau}_1^{(-\theta)} + \alpha_{23(12)}^2 e^{i\mathcal{H}_{2(1)}t} \boldsymbol{\tau}_c^{(\dagger)} e^{-i\mathcal{H}_{1(2)}t} \boldsymbol{\tau}_c^{\dagger(\cdot)} \right),$$

and map this to its 13- (and 31-) counterpart, viz.,

$$\mathbf{V}_{bb(ss)}^{13} = \frac{\alpha_{12}^2 \alpha_{23}^2}{\lambda^4} \left( e^{i\mathcal{H}_{2(1)}t} \boldsymbol{\tau}_1^{(-\theta)} e^{-i\mathcal{H}_{2(1)}t} \boldsymbol{\tau}_1^{(-\theta)} - e^{i\mathcal{H}_2t} \boldsymbol{\tau}_c^{(\dagger)} e^{-i\mathcal{H}_{1(2)}t} \boldsymbol{\tau}_c^{\dagger(\cdot)} \right).$$

Equation (C6) results from Eq. (C3) via this map.

#### d. $\sigma^{22}$ tensor

By inspection of  $\mathbf{V}_{\eta\eta}^{22}$ , we notice that  $\sigma^{22}$  is identical to  $\sigma_{BL}^{22}$  according to

$$(\sigma_{BL,\nu\nu'}^{22})_K = -C_0 \frac{e^2}{i\hbar(\omega + i\delta)} \sum_{bb'} (f_b - f_{b'}) \times \frac{\langle b|\tau_{2\nu}|b'\rangle \langle b'|\tau_{2\nu'}|b\rangle}{\omega + \omega_{bb'} + i\delta}, \quad (\text{C31})$$

which comes from Eq. (C24) after the replacement of matrix  $\boldsymbol{\tau}_1$  by  $\boldsymbol{\tau}_2$ . The resulting expression for  $\sigma^{22}$  depends on  $\alpha_{12,23}$  through the effective Hamiltonian  $\mathcal{H}_2$ . The  $2 \times 2$  matrix  $\sigma^{22} = \sigma_{BL}^{22}$  is diagonal, as is  $\sigma_{BL}^{11}$ . Thus, we obtain Eq. (C8). Furthermore, the nonzero (diagonal) elements of  $\sigma_{BL}^{22}$  come from  $\sigma_e^{(2)}$  with replacement of  $\varphi_{1,2}$  by  $\chi_{1,2}$ . Hence, we obtain

$$\sigma_{BL,xx}^{22} = \sigma_{BL,yy}^{22} = -i2C_0g_v \frac{e^2}{\hbar(\omega + i\delta)} \sum_{bb'} (f_b - f_{b'}) \times \frac{\omega_{bb'}}{(\omega + i\delta)^2 - \omega_{bb'}^2} |\langle \chi_{b1} | \chi_{b'2} \rangle|^2 = \sigma_0^{22} = \sigma_e^{(2)}.$$

We assumed  $|\langle \chi_{b1} | \chi_{b'2} \rangle| = |\langle \varphi_{b1} | \varphi_{b'2} \rangle|$ , since  $\mathcal{H}_{2,K}$  is invariant under the simultaneous operations of layer switch, complex conjugation, and  $x$ -direction reversal.

#### e. $\sigma^{23}$ , $\sigma^{32}$ and $\sigma^{33}$ tensors

Evidently,  $\mathbf{V}_{\eta\eta}^{23,32}$  come from  $\mathbf{V}_{\eta\eta}^{21,12}$  under the replacement of  $\alpha_{12}$  with  $\alpha_{23}$ . By a rescaling and transposition of formula (C5), we readily obtain Eq. (C9). Recall that time reversal symmetry dictates  $\sigma_{BL}^{12}(\omega) = \sigma_{BL}^{21}(\omega)^T$ . Hence, each of  $\sigma^{23,32}(\omega)$  includes the chirality effect via the scalar function  $\sigma_{e,xy}^{12}(\omega)$ .

Regarding  $\sigma^{33}$ , notice that  $\mathbf{V}_{\eta\eta}^{33}$  results from  $\mathbf{V}_{\eta\eta}^{11}$  by switch of the parameters  $\alpha_{12}$  and  $\alpha_{23}$ . This implies that Eq. (C3) yields Eq. (C10). Hence, matrix  $\sigma^{33}$  is diagonal. We set  $\sigma^{33} = \text{diag}(\sigma_0^{33}, \sigma_0^{33})$  where the scalar  $\sigma_0^{33}(\omega)$  directly comes from  $\sigma_0^{11}(\omega)$  by the interchange of  $\alpha_{12}$  and  $\alpha_{23}$ ; cf. Eqs. (C11) and (C15).

\* diom@umd.edu

† tobias.stauber@csic.es

<sup>1</sup> Y. Cao, V. Fatemi, A. Demir, S. Fang, S. L. Tomarken, J. Y. Luo, J. D. Sanchez-Yamagishi, K. Watanabe, T. Taniguchi, E. Kaxiras, R. C. Ashoori, and P. Jarillo-Herrero, *Nature* **556**, 80 (2018).

<sup>2</sup> Y. Cao, V. Fatemi, S. Fang, K. Watanabe, T. Taniguchi, E. Kaxiras, and P. Jarillo-Herrero, *Nature* **556**, 43 (2018).

<sup>3</sup> A. L. Sharpe, E. J. Fox, A. W. Barnard, J. Finney, K. Watanabe, T. Taniguchi, M. A. Kastner, and D. Goldhaber-Gordon, *Science* **365**, 605 (2019).

<sup>4</sup> A. L. Sharpe, E. J. Fox, A. W. Barnard, J. Finney, K. Watanabe, T. Taniguchi, M. A. Kastner, and D. Goldhaber-Gordon, *Nano Letters* **21**, 4299 (2021).

<sup>5</sup> P. J. Ledwith, G. Tarnopolsky, E. Khalaf, and A. Vishwanath, *Phys. Rev. Res.* **2**, 023237 (2020).

<sup>6</sup> Y. Xie, A. T. Pierce, J. M. Park, D. E. Parker, E. Khalaf, P. Ledwith, Y. Cao, S. H. Lee, S. Chen, P. R. Forrester, K. Watanabe, T. Taniguchi, A. Vishwanath, P. Jarillo-Herrero, and A. Yacoby, *Nature* **600**, 439 (2021).

<sup>7</sup> A. T. Pierce, Y. Xie, J. M. Park, E. Khalaf, S. H.

Lee, Y. Cao, D. E. Parker, P. R. Forrester, S. Chen, K. Watanabe, T. Taniguchi, A. Vishwanath, P. Jarillo-Herrero, and A. Yacoby, *Nat. Phys.* **17**, 1210 (2021).

<sup>8</sup> E. Suárez Morell, J. D. Correa, P. Vargas, M. Pacheco, and Z. Barticevic, *Phys. Rev. B* **82**, 121407 (2010).

<sup>9</sup> R. Bistritzer and A. H. MacDonald, *Proc. Natl. Acad. Sci. (USA)* **108**, 12233 (2011).

<sup>10</sup> E. Y. Andrei and A. H. MacDonald, *Nat. Mater.* **19**, 1265 (2020).

<sup>11</sup> C. Jin, E. C. Regan, D. Wang, M. Iqbal Bakti Utama, C.-S. Yang, J. Cain, Y. Qin, Y. Shen, Z. Zheng, K. Watanabe, T. Taniguchi, S. Tongay, A. Zettl, and F. Wang, *Nat. Phys.* **15**, 1140 (2019).

<sup>12</sup> Y. Shimazaki, I. Schwartz, K. Watanabe, T. Taniguchi, M. Kroner, and A. Imamoğlu, *Nature* **580**, 472 (2020).

<sup>13</sup> L. Wang, E.-M. Shih, A. Ghiotto, L. Xian, D. A. Rhodes, C. Tan, M. Claassen, D. M. Kennes, Y. Bai, B. Kim, K. Watanabe, T. Taniguchi, X. Zhu, J. Hone, A. Rubio, A. N. Pasupathy, and C. R. Dean, *Nat. Mater.* **19**, 861 (2020).

<sup>14</sup> X. Wang, C. Xiao, H. Park, J. Zhu, C. Wang, T. Taniguchi, K. Watanabe, J. Yan, D. Xiao, D. R.

- Gamelin, W. Yao, and X. Xu, *Nature* **604**, 468 (2022).
- <sup>15</sup> H. Park, J. Cai, E. Anderson, Y. Zhang, J. Zhu, X. Liu, C. Wang, W. Holtzmann, C. Hu, Z. Liu, T. Taniguchi, K. Watanabe, J.-H. Chu, T. Cao, L. Fu, W. Yao, C.-Z. Chang, D. Cobden, D. Xiao, and X. Xu, *Nature* **622**, 74 (2023).
- <sup>16</sup> H. Park, J. Zhu, X. Wang, Y. Wang, W. Holtzmann, T. Taniguchi, K. Watanabe, J. Yan, L. Fu, T. Cao, D. Xiao, D. R. Gamelin, H. Yu, W. Yao, and X. Xu, *Nat. Phys.* **19**, 1286 (2023).
- <sup>17</sup> Y.-M. Wu, Z. Wu, and H. Yao, *Phys. Rev. Lett.* **130**, 126001 (2023).
- <sup>18</sup> J. Yu, J. Herzog-Arbeitman, M. Wang, O. Vafek, B. A. Bernevig, and N. Regnault, *Phys. Rev. B* **109**, 045147 (2024).
- <sup>19</sup> J. M. Park, Y. Cao, L.-Q. Xia, S. Sun, K. Watanabe, T. Taniguchi, and P. Jarillo-Herrero, *Nat. Mater.* **21**, 877 (2022).
- <sup>20</sup> P. J. Ledwith, A. Vishwanath, and E. Khalaf, *Phys. Rev. Lett.* **128**, 176404 (2022).
- <sup>21</sup> J. M. Park, Y. Cao, K. Watanabe, T. Taniguchi, and P. Jarillo-Herrero, *Nature* **590**, 249 (2021).
- <sup>22</sup> Z. Hao, A. M. Zimmerman, P. Ledwith, E. Khalaf, D. H. Najafabadi, K. Watanabe, T. Taniguchi, A. Vishwanath, and P. Kim, *Science* **371**, 1133 (2021).
- <sup>23</sup> Y. Cao, J. M. Park, K. Watanabe, T. Taniguchi, and P. Jarillo-Herrero, *Nature* **595**, 526 (2021).
- <sup>24</sup> S. Carr, C. Li, Z. Zhu, E. Kaxiras, S. Sachdev, and A. Kruchkov, *Nano Letters* **20**, 3030 (2020).
- <sup>25</sup> Z. Zhu, S. Carr, D. Massatt, M. Luskin, and E. Kaxiras, *Phys. Rev. Lett.* **125**, 116404 (2020).
- <sup>26</sup> A. Ramires and J. L. Lado, *Phys. Rev. Lett.* **127**, 026401 (2021).
- <sup>27</sup> V. T. Phong, P. A. Pantaleón, T. Cea, and F. Guinea, *Phys. Rev. B* **104**, L121116 (2021).
- <sup>28</sup> X. Zhang, K.-T. Tsai, Z. Zhu, W. Ren, Y. Luo, S. Carr, M. Luskin, E. Kaxiras, and K. Wang, *Phys. Rev. Lett.* **127**, 166802 (2021).
- <sup>29</sup> F. Xie, N. Regnault, D. Călugăru, B. A. Bernevig, and B. Lian, *Phys. Rev. B* **104**, 115167 (2021).
- <sup>30</sup> A. Fischer, Z. A. H. Goodwin, A. A. Mostofi, J. Lischner, D. M. Kennes, and L. Klebl, *npj Quantum Mater.* **7**, 5 (2022).
- <sup>31</sup> M. Christos, S. Sachdev, and M. S. Scheurer, *Phys. Rev. X* **12**, 021018 (2022).
- <sup>32</sup> S. Turkel, J. Swann, Z. Zhu, M. Christos, K. Watanabe, T. Taniguchi, S. Sachdev, M. S. Scheurer, E. Kaxiras, C. R. Dean, and A. N. Pasupathy, *Science* **376**, 193 (2022).
- <sup>33</sup> X. Liu, N. J. Zhang, K. Watanabe, T. Taniguchi, and J. I. A. Li, *Nat. Phys.* **18**, 522 (2022).
- <sup>34</sup> J.-X. Lin, P. Siriviboon, H. D. Scammell, S. Liu, D. Rhodes, K. Watanabe, T. Taniguchi, J. Hone, M. S. Scheurer, and J. I. A. Li, *Nat. Phys.* **18**, 1221 (2022).
- <sup>35</sup> M. Christos, S. Sachdev, and M. S. Scheurer, *Nat. Commun.* **14**, 7134 (2023).
- <sup>36</sup> J. González and T. Stauber, *Nat. Commun.* **14**, 2746 (2023).
- <sup>37</sup> T. Devakul, P. J. Ledwith, L.-Q. Xia, A. Uri, S. C. de la Barrera, P. Jarillo-Herrero, and L. Fu, *Science Advances* **9**, eadi6063 (2023).
- <sup>38</sup> H. Kim, Y. Choi, É. Lantagne-Hurtubise, C. Lewandowski, A. Thomson, L. Kong, H. Zhou, E. Baum, Y. Zhang, L. Holleis, K. Watanabe, T. Taniguchi, A. F. Young, J. Alicea, and S. Nadj-Perge, *Nature* **623**, 942 (2023).
- <sup>39</sup> S. Becker, M. Embree, J. Wittsten, and M. Zworski, *Prob. Math. Phys.* **3**, 69 (2022).
- <sup>40</sup> N. Nakatsuji, T. Kawakami, and M. Koshino, *Phys. Rev. X* **13**, 041007 (2023).
- <sup>41</sup> F. K. Popov and G. Tarnopolsky, *Phys. Rev. Res.* **5**, 043079 (2023).
- <sup>42</sup> A. Uri, S. C. de la Barrera, M. T. Randeria, D. Rodan-Legrain, T. Devakul, P. J. D. Crowley, N. Paul, K. Watanabe, T. Taniguchi, R. Lifshitz, L. Fu, R. C. Ashoori, and P. Jarillo-Herrero, *Nature* **620**, 762 (2023).
- <sup>43</sup> L.-Q. Xia, S. C. de la Barrera, A. Uri, A. Sharpe, Y. H. Kwan, Z. Zhu, K. Watanabe, T. Taniguchi, D. Goldhaber-Gordon, L. Fu, T. Devakul, and P. Jarillo-Herrero, arXiv:2310.12204.
- <sup>44</sup> A. Ceferino and F. Guinea, *2D Mater.* **11**, 035015 (2024).
- <sup>45</sup> E. Khalaf, A. J. Kruchkov, G. Tarnopolsky, and A. Vishwanath, *Phys. Rev. B* **100**, 085109 (2019).
- <sup>46</sup> T. Stauber, T. Low, and G. Gómez-Santos, *Phys. Rev. Lett.* **120**, 046801 (2018).
- <sup>47</sup> Within the continuum description, the in-plane magnetization  $m_{\parallel} = e\xi \times \mathbf{e}_z$  is defined with respect to the dipolar current via the sheet current  $\mathbf{j}(z)$  as  $\xi = \int dz z \mathbf{j}(z)$ .<sup>48</sup> Obviously,  $\xi$  and thus  $m_{\parallel}$  vanishes for  $\mathbf{j}(z) = \mathbf{j}(-z)$ .
- <sup>48</sup> D. Guerzi, P. Simon, and C. Mora, *Phys. Rev. B* **103**, 224436 (2021).
- <sup>49</sup> T. Stauber, M. Wackerl, P. Wenk, D. Margetis, J. González, G. Gómez-Santos, and J. Schliemann, *Small Sci.* **3**, 2200080 (2023).
- <sup>50</sup> M. Sánchez-Sánchez, I. Díaz, J. González, and T. Stauber, e-print, arXiv:2403.03140v2 [cond-mat.mes-hall] (2024).
- <sup>51</sup> G. Gómez-Santos and T. Stauber, *Phys. Rev. Lett.* **106**, 045504 (2011).
- <sup>52</sup> T. Stauber and H. Kohler, *Nano Lett.* **16**, 6844 (2016).